Scilight

Photochemistry and Spectroscopy

https://www.sciltp.com/journals/ps

Review

Check for updates

Intensity Calibration of Raman Instruments: A Review †

Roberto Pilot

Department of Chemical Sciences and INSTM Research Unit, University of Padova, Via Marzolo 1, 35131 Padova, Italy; roberto.pilot@unipd.it

† This article is dedicated to Prof. Giuseppe Zerbi in recognition of his outstanding scientific contributions to Spectroscopy.

How To Cite: Pilot, R. Intensity Calibration of Raman Instruments: A Review. *Photochemistry and Spectroscopy* **2026**, *2*(2), 7. https://doi.org/10.53941/ps.2026.100018

Received: 30 November 2025
Revised: 19 March 2026
Accepted: 24 March 2026
Published: 13 May 2026

Abstract: Raman spectroscopy is a powerful analytical technique widely used in many scientific fields due to its molecular fingerprinting capabilities and non-destructive nature. However, the recorded Raman spectrum is strongly dependent on the characteristics of the instrument and on the experimental configuration: in particular, the relative intensities of Raman bands can vary substantially between instruments, limiting reproducibility and accuracy. Intensity-calibrated spectra are therefore increasingly needed, as their availability would facilitate studies based on band intensity ratios, the building of unified spectral databases, and the inter-instrument transferability of chemometric and machine learning models. This review provides an overview of the methods available for the intensity calibration of Raman spectrometers. After introducing the definition of the instrument response function and the required spectral transformations, we examine calibration approaches based on broadband lamps, luminescent materials (certified and non-certified), and Raman scatterers, discussing their experimental implementation, advantages and limitations. Insights from interlaboratory comparison studies are also reviewed, demonstrating that inter-instrument variability remains substantial, and highlighting the importance of intensity calibration. Finally, since inter-instrument transferability can be addressed both by physically calibrating the instrument response and through data-processing strategies known as calibration transfer methods, a brief overview of the latter is also included, as the two approaches are complementary and inherently intertwined.

Keywords: Raman; intensity calibration; instrument response function; machine learning; model transfer

1. Introduction

Raman spectroscopy is a powerful and versatile technique that, owing to its fingerprint-recognition capabilities and non-destructive nature, enables the characterization and identification of materials in diverse scientific and industrial applications [1,2]. Its fields of application include: the pharmaceutical sector [3,4], for example in studying drug formulations [5] and investigating different polymorphic forms [6]; the characterization of 2D materials [7], carbon-based materials [8–10] and polymers [11–13]; forensic science [14]; cultural heritage [15–17]; geology [18]; and planetary exploration studies [19]. A common variation of conventional spontaneous Raman spectroscopy is Surface-Enhanced Raman Spectroscopy (SERS) [20–25], which, owing to the field-localization effect of plasmonic substrates, can enhance the inherently weak Raman signal by many orders of magnitude. Combining high sensitivity with fingerprint recognition capabilities, SERS has found applications in various fields like environmental monitoring [26,27], food safety [28], biomedicine [29–31], catalysis [32], and art preservation [33]. It is also worth mentioning Spatially Offset Raman Spectroscopy (SORS), [34,35] which enables the analysis of materials located beneath surfaces by minimizing the Raman signal originating from the

surface itself: for example, the identification of pharmaceutical products through their packaging [36] and the detection of liquid explosives contained in bottles or other containers [37].

Despite its broad use, Raman spectroscopy still faces significant challenges in terms of reproducibility and accuracy. The recorded spectrum, in particular the wavenumber positions, bandwidths, and relative intensities of Raman bands, depends strongly on the characteristics of the instrument and on the specific experimental configuration used [38]. These issues are generally more pronounced in dispersive Raman spectroscopy than in Fourier Transform Infrared (FTIR) spectroscopy, where the wavenumber scale is intrinsically standardized through interferometric laser calibration and the intensity scale is relative, therefore naturally compensating for variations in the instrumental response [38,39]. Calibration is therefore essential in Raman spectroscopy for improving inter-instrument comparability.

Wavenumber calibration is relatively straightforward and widely implemented. Commercial Raman spectrometers are factory-calibrated; however, discrepancies of several wavenumbers (often exceeding ±5 cm^{-1}) may arise if no periodic recalibration is performed. Such deviations can originate from mechanical drift, optical misalignment, or drifts in the excitation laser wavelength. Wavenumber calibration is typically carried out using reference materials with well-known Raman band positions, such as single-crystal silicon [40] or other compounds (e.g., naphthalene, polystyrene, benzonitrile, and cyclohexane), whose Raman shifts are known to within 0.1–2 cm^{-1} across the 85–3327 cm^{-1} range [38,41].

Bandwidth calibration is probably the least commonly performed. The measured Raman band shape results from the convolution of the true spectral profile of the sample with the instrument response, which is not infinitely narrow because of its finite resolution [42]. Recovering the true line shape requires measuring the response of the instrument using a source with spectral lines much narrower than the spectrometer resolution, like plasma emission lines of a gas laser, and subsequently applying deconvolution procedures [43–45]. Bandwidth calibration is generally applied only in specific studies where accurate linewidth determination is essential [45].

Intensity calibration is rarely implemented in practice. The measured Raman spectrum is always distorted relative to the true Raman spectrum of the sample due to the wavelength-dependent and polarization-dependent response of the optical components and of the detector (this instrumental contribution is normally referred to as the instrument response function, IRF). As a consequence, spectra acquired with different instruments, or with the same instrument under different configurations, can exhibit significantly different relative intensities. While this does not hinder applications based solely on band positions, it can become a limitation in other cases: for example, when determining the cross-section of a Raman band relative to a reference with a known cross-section, when quantitative measurements are performed [46,47], or when physical or chemical properties are inferred from specific intensity ratios (e.g., the degree of disorder in carbon materials [10], the crystallinity and copolymer composition in polymers [11]). Reported procedures in the literature rely on the use of known emission spectra produced either by tungsten-halogen lamps or luminescent materials, which can be used to determine the IRF and subsequently correct the measured sample spectrum [38,48].

The possibility of generating instrument-independent spectra is highly desirable in the rapidly growing field of machine learning applied to Raman spectroscopy [49–52]: these methods have been successfully applied to the recognition and differentiation of species whose spectral differences are subtle and difficult to recognize by traditional inspection methods, like viruses [53], bacteria [54] and breast cancer subtypes [55]. Instrument-independent spectra, containing only the intrinsic chemical and physical information of the material, would favour the creation of unified spectral databases, which is expected to significantly facilitate machine learning algorithm performance, both during the training phase and when analysing unknown spectra [56,57]. Furthermore, chemometric and machine learning models developed on one instrument could in principle be directly applied to spectra acquired on another. It is worth mentioning that data-processing strategies, commonly referred to as calibration transfer methods, also exist to address inter-instrument model transferability [58–62]. They can either be used in combination with physical calibration of the instrument response to compensate for residual inter-instrument differences, or applied independently to non-calibrated spectra.

To the best of our knowledge, the topic of Raman intensity calibration methods has been reported only in a few reviews. Jakubek et al. [45] provided an overview of the calibration of all three parameters (wavenumber, bandwidth, and intensity) but specifically in the context of astromaterials and planetary science. Ntziouni et al. [63] published a comprehensive analysis focused on listing and classifying the existing official standards and guides for Raman spectroscopy.

This paper aims to provide a general methodological review of the techniques proposed for intensity calibration, which remains largely unemployed in practice, despite its relevance and potential impact on a broad range of scientific applications. We first outline the overall workflow of Raman data analysis to contextualize where the intensity calibration step is placed. We then summarize methods based on broadband lamps and certified

Standard Reference Materials (SRMs), which represent the gold standard; since SRMs are not so widely available, we also examine the use of non-certified reference materials. Finally, as intensity calibration and calibration transfer methods represent complementary strategies for achieving inter-instrument comparability, a brief overview of calibration transfer methods is also provided.

2. Workflow of Raman Data Analysis

It is worth describing the overall workflow involved in Raman data analysis, from the design of experiment (DoE) to advanced data analysis, in order to clarify where intensity calibration and calibration transfer fit in this sequence. An overview of this workflow is shown in Figure 1, reproduced from Ref. [64]: a brief description of the steps is provided in Table 1. As illustrated, intensity calibration belongs to the data preprocessing stage, whereas calibration transfer belongs to the modeling stage, and occurs after the model has been developed.

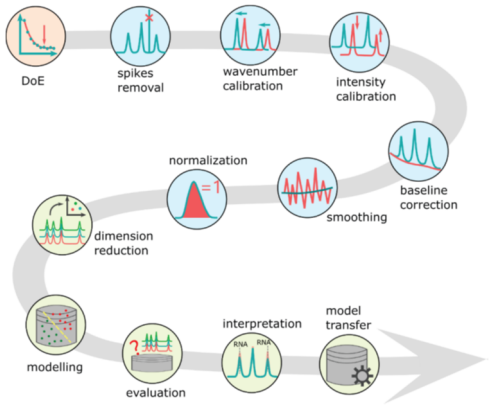

Figure 1. The key steps of Raman data analysis. Steps are briefly explained in Table 1. Reproduced with permission from Guo et al. [64]. DoE stands for Design of Experiment.

Table 1. Brief description of the steps involved in the workflow of Raman data analysis [64].

Operation	Description
Design of experiment	
Sample size planning	Determination of the minimum sample size needed to achieve reliable results
Preprocessing	
Spike removal	Removal of sharp intensity spikes caused by cosmic rays hitting the detector
Wavenumber calibration	Correction of the Raman shift axis using known reference band positions.
Intensity calibration	*Correction of the wavelength-dependent instrument response*
Baseline correction	Removal of slowly varying background contributions like fluorescence
Smoothing	Reduction of high-frequency noise
Normalization	Rescaling of spectral intensities to compensate for variations in excitation power or other measurement conditions
Data Modeling	
Dimension reduction	Transformation of spectral data into a smaller set of variables that retain the most relevant information
Model construction	Development of a model to extract chemical or physical information from spectra
Model evaluation	Evaluation of model performance on independent datasets
Model interpretation	Identification of spectral variables that contribute most significantly to the model and linking them to chemical information
Calibration transfer	Adaptation of a model developed on one instrument so that it can be applied to spectra acquired with another instrument

3. Basic Framework of Raman Intensity Calibration

3.1. Origin of Spectral Distortion

As mentioned in the introduction, the true Raman signal emitted by a sample is modified along the optical path to the detector. These distortions arise from the wavelength and polarization dependent transmission and

reflectance of all optical components, in particular the diffraction gratings, as well as from the wavelength dependent quantum efficiency of the detector. Figure 2a,b show representative examples of the spectral response of a grating (Adar et al. [65]) and of a charge-coupled device (CCD) detector, respectively. Since tracking the wavelength and polarization dependence of every component present in the optical path is impractical, calibration procedures rely on the use of a reference spectrum whose normalized intensity as a function of wavelength is known, either from first principles modeling or from prior characterization. Tungsten-halogen lamps and luminescent materials are commonly used for this purpose, although Raman spectra with known band-intensity ratios may also serve as references.

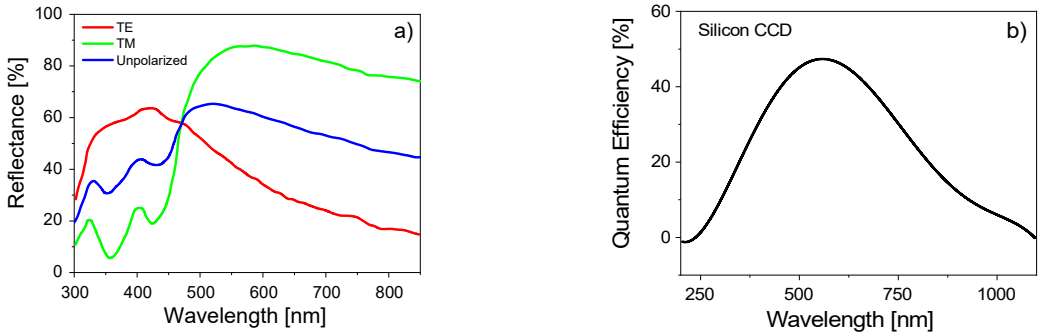

Figure 2. (**a**) Example of the reflectivity of a diffraction grating as a function of wavelength, for transverse electric (TE, electric field parallel to the grooves), transverse magnetic (TM, electric field perpendicular to the grooves) polarization, and for unpolarized light. Adapted with permission from Adar et al. [65]; (**b**) Typical quantum efficiency of a front illuminated silicon CCD.

3.2. Definition of the Instrument Response Function

Let us consider a reference source (to fix ideas a broadband lamp) with a known emission spectrum, $\Phi_L(\Delta\tilde{\nu})$, where $\Delta\tilde{\nu}$ is the Raman shift calculated with respect to the absolute wavenumber of the excitation laser. When the spectrum of this reference source is recorded with the Raman spectrometer, the measured spectrum, $S_L(\Delta\tilde{\nu})$, will be the product of the true spectrum $\Phi_L(\Delta\tilde{\nu})$ and the IRF, $R(\Delta\tilde{\nu})$ [38,48]:

$$S_L(\Delta\tilde{\nu}) = R(\Delta\tilde{\nu})\Phi_L(\Delta\tilde{\nu}) \quad (1)$$

From this equation, $R(\Delta\tilde{\nu})$ can therefore be determined experimentally. When the spectrum of a sample is recorded, its measured spectrum $S_S(\Delta\tilde{\nu})$ will be the product of its true spectrum $\Phi_S(\Delta\tilde{\nu})$ and the same IRF:

$$S_S(\Delta\tilde{\nu}) = R(\Delta\tilde{\nu})\Phi_S(\Delta\tilde{\nu}) \quad (2)$$

By inserting the expression of $R(\Delta\tilde{\nu})$ obtained from Equation (1) into (2), the true sample spectrum turns out to be:

$$\Phi_S(\Delta\tilde{\nu}) = \frac{\Phi_L(\Delta\tilde{\nu})}{S_L(\Delta\tilde{\nu})} S_S(\Delta\tilde{\nu}) \quad (3)$$

It should be noted that this procedure yields a relative correction of the instrument's spectral response, valid within the spectral range covered by the emission of the reference source $\Phi_L(\Delta\tilde{\nu})$. Since $\Phi_L(\Delta\tilde{\nu})$ is typically provided over a discrete set of wavenumber values, it is often fitted with a smooth polynomial function so that it can be recalculated using the exact spacing of the instrument spectral axis. Figure 3 summarizes the procedure described above. The known irradiance of the lamp is normally given in units $\left[\frac{Watt}{cm^2 * nm}\right]$ [66]: however, Raman spectra are recorded in different units and therefore conversion is required so the quantities that appear in Equation (3) are homogeneous, as explained in the following sections.

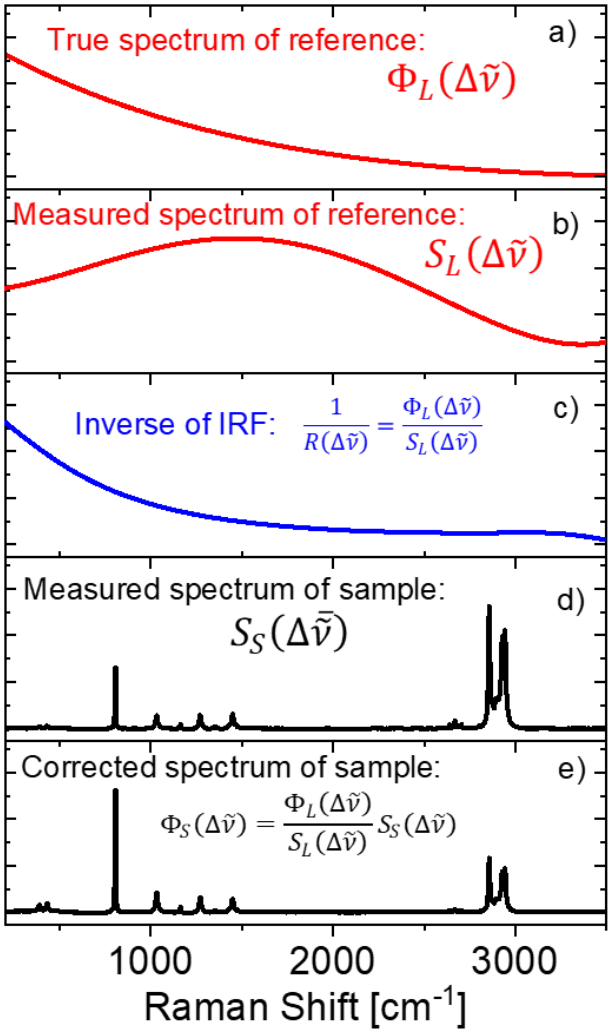

Figure 3. Steps involved in the intensity calibration procedure. From top to bottom: (**a**) True spectrum of the reference; (**b**) Measured spectrum of the reference; (**c**) Calculated IRF; (**d**) Measured spectrum of the sample; and (**e**) Corrected spectrum of the sample.

3.3. Power to Photon Count Conversion

Raman spectrometers are generally equipped with CCD detectors, whose signal is proportional to the number of detected photons rather than to optical power (measured in Watt). In order to convert Watt to $\frac{photons}{s}$, the irradiance must be divided by the photon energy, that is multiplied by $\lambda\frac{10^{-9}}{hc}$ where $\lambda[nm]$ is the wavelength, $h[J*s]$ is the Planck constant and $c[\frac{m}{s}]$ is the speed of light. Note that the factor $\frac{10^{-9}}{h\,c}$ is a constant and will multiply the entire reference spectrum by the same amount, but without changing its shape.

3.4. Jacobian Transformation

Spectrographs disperse light almost linearly in wavelength [38,67], meaning that each CCD pixel corresponds to a nearly constant wavelength interval. Consequently, raw spectral intensities are effectively recorded per unit wavelength. Raman spectra, however, are conventionally expressed in terms of $\Delta\tilde{\nu}$. Since absolute wavenumber $\tilde{\nu}[cm^{-1}]$ and wavelength $\lambda[nm]$ are related by

$$\tilde{\nu} = \frac{10^7}{\lambda} \tag{4}$$

the two scales are nonlinear with respect to each other. As a consequence, although the wavelength interval per CCD pixel is constant, the corresponding wavenumber interval changes significantly across the Raman spectrum. When the abscissa is converted from wavelength to wavenumber, the ordinate must also be transformed. This correction is necessary to ensure that the total number of photons collected (the area under the spectrum) remains the same, independently of whether the spectrum is expressed as a function of wavenumber or wavelength. This

process of transforming the ordinate to account for the change in the abscissa scale is referred to as the Jacobian correction or Jacobian transformation. It is well known in the context of photoluminescence [68]; concerning Raman spectroscopy, it has been discussed in the context of intensity calibration procedures [66,69,70].

To derive the transformation, let's consider an experimental spectrum recorded as a function of wavelength, $S(\lambda)$. When one expresses it as a function of wavenumber, $S'(\tilde{\nu})$, the total number of photons within an infinitesimal interval must remain the same independently of the choice of abscissa. Therefore, for an infinitesimal interval:

$$S'(\tilde{\nu})d\tilde{\nu} = S(\lambda)d\lambda \tag{5}$$

Differentiating both sides of Equation (4) with respect to wavelength gives:

$$\frac{d\tilde{\nu}}{d\lambda} = -\frac{10^7}{\lambda^2} \tag{6}$$

Combining Equations (5) and (6) results:

$$S'(\tilde{\nu}) = S(\lambda)\left|\frac{d\lambda}{d\tilde{\nu}}\right| = S(\lambda)\,\frac{\lambda^2}{10^7} \tag{7}$$

The negative sign in (6) simply reflects that wavelength decreases as wavenumber increases, therefore the absolute value is used in Equation (7). This equation states that when the abscissa is converted to wavenumber the ordinate has to be corrected by a factor $\frac{\lambda^2}{10^7}$. This transformation is graphically illustrated in Figure 4.

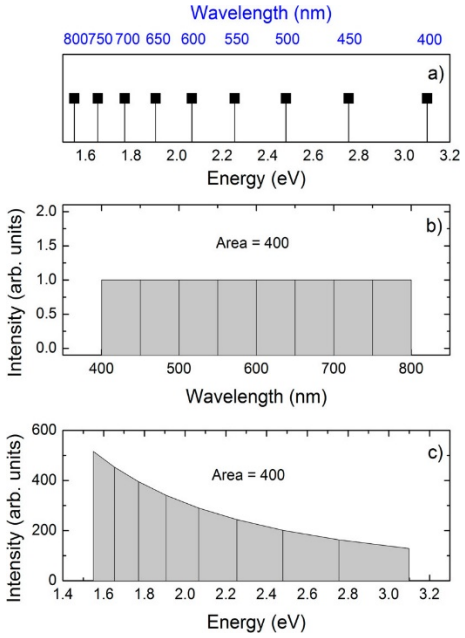

Figure 4. (**a**) Data that are evenly spaced in wavelength (nm) are not evenly spaced in energy (eV); (**b**) A spectrum with constant intensity 1 between 400 and 800 nm has an area of 400; (**c**) When the abscissa is converted to energy, the ordinate transforms as well to preserve the area of the spectrum. The signal per unit energy is higher at lower energy. Reproduced with permission from Ref. [68].

Numerical Examples of the Jacobian Correction

The following numerical example demonstrates how the Jacobian correction can substantially influence the band intensity ratios in Raman spectra. Consider a Raman spectrum excited at λ_{ex} = 532 nm and two bands at $\Delta\tilde{\nu}_1$ = 3000 cm^{-1} (λ_1 = 633.0 nm absolute wavelength) $\Delta\tilde{\nu}_2$ = 300 cm^{-1} (λ_2 = 540.6 nm absolute wavelength). Their intensity ratio is expressed as:

$$\frac{S\prime(\Delta\tilde{\nu}_1)}{S\prime(\Delta\tilde{\nu}_2)} = \frac{\lambda_1^2}{\lambda_2^2}\frac{S(\lambda_1)}{S(\lambda_2)} \tag{8}$$

$$\left(\frac{I(Ex{=}532\ nm;\,\Delta\tilde{\nu}_1)}{I(Ex{=}532\ nm;\,\Delta\tilde{\nu}_2)}\right)_{corrected} = 1.37\left(\frac{I(Ex{=}532\ nm;\,\Delta\tilde{\nu}_1)}{I(Ex{=}532\ nm;\,\Delta\tilde{\nu}_2)}\right)_{non\ corrected} \tag{9}$$

With λ_{ex} = 785 nm and the same bands at 3000 cm^{-1} (λ_1 = 1026.8 nm absolute wavelength) and 300 cm^{-1} (λ_2=803.9 nm absolute wavelength) the intensity ratio results

$$\left(\frac{I(Ex=785\ nm;\Delta\tilde{\nu}_1)}{I(Ex=785\ nm;\Delta\tilde{\nu}_2)}\right)_{corrected} = 1.63\left(\frac{I(Ex=785\ nm;\Delta\tilde{\nu}_1)}{I(Ex=785\ nm;\Delta\tilde{\nu}_2)}\right)_{non\ corrected} \quad (10)$$

This correction is therefore significant and has to be included in the calibration procedure. Figure 5 shows the Jacobian correction as a function of Raman shift for the four most common excitation wavelengths: 532, 633, 785 and 1064 nm. To highlight its spectral dependence, the correction is normalized to one at zero Raman shift.

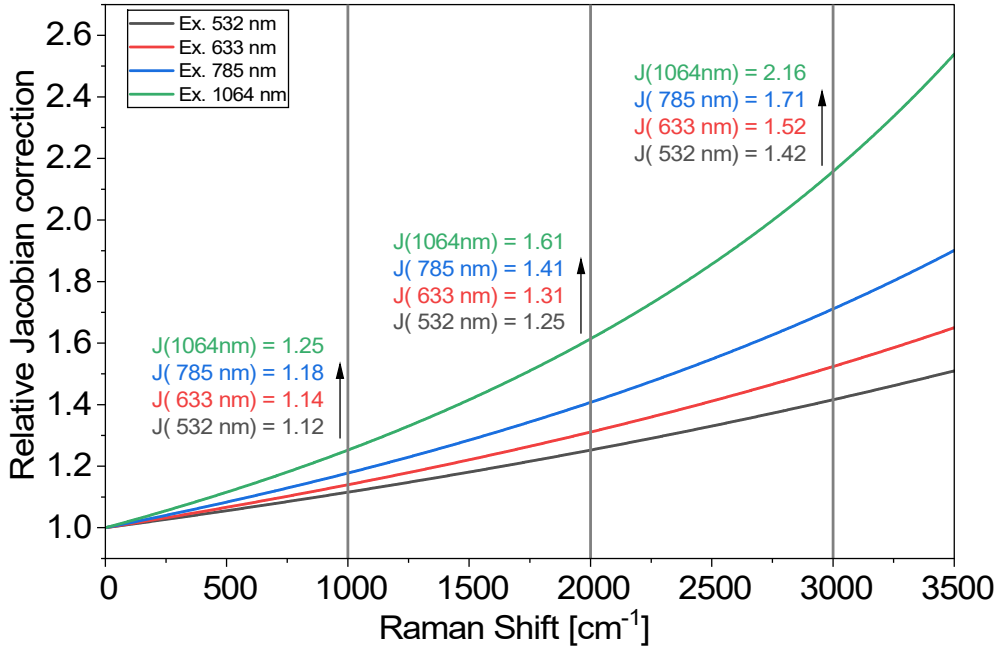

Figure 5. Jacobian correction (J) normalized to one at zero Raman shift, as a function of Raman shift, for excitation wavelengths at 532, 633, 785 and 1064 nm. Vertical bars indicate the positions at 1000, 2000 and 3000 cm^{-1}, where numerical values of J are reported.

3.5. The Combined Correction Factor

In summary, to obtain the correct units for Raman intensity calibration, the lamp irradiance must be converted from $\left[\frac{Watt}{cm^2*nm}\right]$ to $\left[\frac{photons}{s*cm^2*cm^{-1}}\right]$. Considering both the power to photon count conversion and the Jacobian transformation, the irradiance must be finally multiplied by:

$$\lambda^3 \frac{10^{-16}}{hc} \propto \lambda^3 \quad (11)$$

Once the reference spectrum has been expressed in the correct units, $\Phi_L(\Delta\tilde{\nu})$, the calibration procedure is straightforward. The Raman spectrum of the sample, $S_S(\Delta\tilde{\nu})$, and the spectrum of the reference lamp, $S_L(\Delta\tilde{\nu})$, are recorded under identical experimental conditions, with the abscissa expressed in cm^{-1} and with no Jacobian correction applied to either measured spectrum. The Jacobian correction is instead incorporated into the known reference spectrum, $\Phi_L(\Delta\tilde{\nu})$, and therefore appears automatically in the corrected sample spectrum $\Phi_S(\Delta\tilde{\nu})$, obtained through Equation (3). Note that, in the procedure above, it is also correct to apply the Jacobian correction to both $S_S(\Delta\tilde{\nu})$ and $S_L(\Delta\tilde{\nu})$: in this case the correction cancels out, since Equation (3) contains their ratio, yielding the same result. As a final note, certified standard reference materials (described in Section 6.1) provide reference spectra that already incorporate both the conversion to $\frac{photons}{s}$ and the Jacobian transformation. When a calibration lamp, a non-certified fluorescent material, or a Raman spectrum is used as reference, the user must verify that the reference spectrum incorporates the appropriate corrections before using Equation (3), depending on the units in which it is provided.

3.6. Remarks on the Implementation of Intensity Calibration

3.6.1. Position of Intensity Calibration in the Workflow of Raman Data Analysis

According to the scheme reported in Section 2, intensity calibration should be performed after wavenumber calibration and before baseline correction. The first point is motivated by the fact that both the sample and reference measured spectra must be properly aligned with the reference standard spectrum to ensure that the intensity calibration is applied at the correct wavenumber positions. Concerning the second point, intensity calibration is a multiplicative operation that scales both the Raman signal and any additive background present in the spectrum. If baseline subtraction is performed first and the background has not been perfectly removed, the residual component will also be scaled by the subsequent intensity calibration, potentially introducing errors. It is therefore preferable to perform baseline subtraction after intensity calibration. It is worth noting that the order of the pre-processing steps (Table 1) is not a rigid linear procedure, since the various steps influence each other. Therefore, although the presented order is probably the most logical one, steps may need to be iteratively repeated based on the outcome of the others [64].

3.6.2. Treatment of Dark Counts, Ambient Light and CCD Readout Bias

Before applying intensity calibration, it is necessary to remove background contributions that do not originate from the sample. These include CCD readout bias, dark current, and ambient light [38]. The CCD readout bias is a positive electronic offset introduced during CCD readout to prevent negative digital values caused by readout noise. Dark current arises from thermally generated electrons that accumulate during the detector integration time and contribute to the measured signal: this contribution is proportional to the integration time. Finally, ambient light may reach the detector due to imperfect optical isolation of the instrument, producing a signal that is also proportional to the integration time.

To remove these non-sample related contributions, a dark spectrum should be recorded with the laser off (using the same integration time as employed for the sample and reference measurements) and subsequently subtracted from them. While these contributions may be negligible (detector cooling strongly reduces the dark current, and ambient light contributions should also be minimal under appropriate experimental conditions) or automatically subtracted by the instrument, their impact should always be verified. The presence of this background can usually be easily recognized in Raman spectra because the baseline is shifted from zero. However, when a fluorescent compound is used as a reference, this is no longer the case; the instrumental background becomes indistinguishable from the true fluorescence, potentially introducing significant errors in the calculation of the IRF.

3.6.3. Signal-to-Noise Considerations

Going towards the long-wavelength region, two phenomena tend to occur simultaneously:

- The signal-to-noise ratio (SNR) tends to decrease. This occurs because fewer electrons (S) are generated by the detector, due both to the reduction of the Raman cross-section and to the decreasing quantum efficiency of silicon-based detectors (in the shot-noise-limited regime, the $SNR \propto \sqrt{S}$) [38].
- The correction due to the IRF becomes larger because of the lower instrument sensitivity.

In this way, intensity calibration can introduce a significant amplification of the noise. As highlighted by Ying et al. [71], machine learning models are highly susceptible to overfitting when dealing with noisy data. By mistaking noise for meaningful features, a model may achieve artificially high accuracy during the training phase while failing to perform well on unseen data. These effects can be mitigated by carrying out appropriate denoising operations after intensity calibration and before model construction, if needed [72].

4. Classification of Calibration Sources

First of all, it is worth distinguishing between a reference material and a standard (or certified) reference material (SRM) [63]. A reference material is any material used for comparison or calibration, but without a formal certification. A SRM, in contrast, is a reference material whose relevant properties have been rigorously measured, validated and certified by a national metrology institute, like the National Institute for Standards and Technology (NIST). In the context of Raman intensity calibration, only the luminescent glass materials provided by NIST are SRMs, designed specifically for calibrating the spectral responsivity of Raman spectrometers at common excitation wavelengths. Other calibration sources (like fluorophores in solution, other luminescent glasses, or

Raman-active liquids) are considered simply as reference materials. Broadband lamps can also be used for intensity calibration and they are available with NIST calibrated irradiance.

The calibration sources studied in the literature are listed below and discussed in detail in the following sections.

- Broadband irradiance-calibrated lamps
- Luminescent materials
  - Luminescent glasses (SRM)
  - Fluorophores in solution or other (non-certified) luminescent glasses
- Raman scatterers
  - Rotational and vibrational-rotational Raman spectra of diatomic gases
  - Raman spectra of organic liquids with known band ratios

5. Calibration with Broadband Lamps

The primary emission standard is a blackbody radiator. It is an ideal radiative source, as it emits thermal radiation with a spectral distribution defined solely by its temperature, in accordance with Planck's law. It consists of a cavity with a small aperture and an internal surface of very high absorptivity (e.g., coated with graphite), which ensures an effective emissivity approaching unity. The cavity is heated to a stable and accurately measured temperature. Because the emitted spectral radiance can be calculated exactly from fundamental physical constants and the measured temperature, the radiation exiting the aperture serves as a primary emission standard for radiometric calibration. A practical example of black body is given in the papers by Palchetti et al. [73] and by Petty et al. [74]. The latter work also provides an example in which a blackbody source was used to calibrate a spectrometer. In this case, the blackbody consisted of an electrically heated tubular furnace filled with firebrick pieces acting as the emissive material, operated at a controlled temperature of about 1300 °C and aligned along the optical axis of the spectrometer.

Blackbody radiators are difficult to use in a standard laboratory since they are cumbersome and need to be heated at high temperature to emit visible light: therefore, they are mainly used in metrology institutes to calibrate tungsten–halogen lamps, which can be used as secondary standards for calibrating Raman instruments as illustrated in the next sections.

5.1. Tungsten-Halogen Lamps

Only a limited number of articles address this topic. Some of them are quite dated, but they provide experimental details on the challenges encountered during calibration. These details can be useful for anyone intending to use this method, and so they are worth analyzing in detail.

5.1.1. Setup with the Lamp Embedded in an Integrating Sphere

Choquette et al. [70] described the procedure used to calibrate three NIST SRMs, namely the luminescent glasses SRM 2241, 2242, and 2243, for excitation wavelengths of 785, 532, and 488/514.5 nm, respectively. They used a NIST-calibrated reference source consisting of a 10 W tungsten-halogen lamp mounted inside an integrating sphere. The sphere's interior surface was coated with Spectralon, a fluoropolymer characterized by extremely high reflectivity across the ultraviolet, visible, and near-infrared regions [75]. Spectralon acts as an almost ideal diffuse reflector, exhibiting near-Lambertian behavior [76]. The main advantage of enclosing the tungsten-halogen lamp within the integrating sphere was that the sphere output provided a constant radiance source, thereby minimizing polarization effects and non-uniform light distribution originating from the lamp filament. The large spectral calibration range (from 400 to 1200 nm) allowed for the calibration of all the luminescent glasses mentioned above. A micro-Raman and two macro-Raman setups were used. In the macro-Raman configurations, a backscattering geometry was achieved by using a small mirror placed in front of the collection lens to direct the laser towards the sample. The laser was delivered either as a collimated beam or focused onto the sample using a cylindrical or spherical lens. The light from the integrating sphere was directed into the instrument using a Spectralon diffuser at the sample position. In the micro-Raman system, a 200 μm pinhole was placed at the focus of the microscope objective and aligned by maximizing the excitation laser throughput. Light from the integrating sphere, propagating parallel to the optical bench, was diffused vertically by a piece of Spectralon, towards the pinhole. In both configurations, the illumination geometry with the white light was aimed to mimic the Raman emission of an actual sample, in order to ensure that they both follow a similar path to the detector.

In all setups, a polarization scrambler was inserted to randomize the polarization of the radiation entering the spectrograph, independently of its origin (white-light source, luminescent glass, or Raman emission).

The impact of the calibration was particularly evident when examining the emission spectra of the glasses. A strong etaloning effect, typical of back-illuminated CCDs, appeared in the uncorrected data, but it was effectively removed after calibration.

5.1.2. Setups with the Lamp in Free Space

Fryling et al. [77] coupled the output of NIST calibrated lamp into an optical fiber through a diffuser and the output of the fiber was placed at the sample position. In this way, the light exiting the fiber mimicked a real sample emission, following the same optical path into the spectrograph and to the CCD detector. The drawback of this method was that, while the lamp emission was calibrated, the fiber output was not, and therefore had to be calibrated in the laboratory. The authors carried out this calibration as follows. First, the tungsten lamp was placed 1 m in front of the spectrograph entrance slit, and its spectrum was recorded. Then, the fiber was positioned 1 cm from the entrance slit with a diffuser placed between them, and its spectrum was recorded. The ratio between the known calibrated emission and the measured lamp spectrum provided the IRF, by means of which the emission from the fiber was calibrated. This paper showed that, after calibration, the ratios among some selected bands of naphthalene measured with excitation at 514.5 nm were much closer to the ratios among the same bands with excitation at 784 nm than before calibration. Similar results were obtained for dichloromethane, confirming the role played by the calibration in reducing instrument-related distortions.

McConkey et al. [78] used calibrated tungsten lamps to determine the spectral response of a photomultiplier tube placed at the exit slit of a monochromator. Their main findings were: (a) when using lamps calibrated by different manufacturers and exposing the entire filament envelope to the entrance slit, the ratio of the photomultiplier signals at a given wavelength differed from the value predicted from the provided calibration spectra by only about 1%. This close agreement confirmed the consistency between the different calibration standards; (b) when using a single lamp in the aperture-limited mode, that is with an aperture was placed in front of it to select only the emission from a 10 mm central region of the filament, the ratio of the signal recorded with and without the aperture differed by about 7% with respect to what expected from calibrated data. This discrepancy was attributed to a temperature gradient along the filament, implying that the true spectral emission varied, depending on which portion of the filament was selected by the aperture.

Malyj et al. [69] studied how different optical setups affect spectrometer calibration. In the direct-view setups (A, B, C, D) the lamp was placed at approximately two meters from the objective lens that, in a normal experiment, collected the Raman signal from a sample and coupled it into the spectrograph; no diffuser was used. The large distance served to send only a small fraction of light emitted from the lamp into the spectrograph in order not to saturate or damage the detector. These arrangements exhibited significantly different measured spectra: (A) without any other optics, characteristic fluctuations in the spectrum were present, which changed reproducibly with small shifts in the lamp position; (B) the insertion of a polarizer and a polarization scrambler introduced a periodic interference pattern; (C) using a lamp with a different filament arrangement provided similar behaviors as in (A) and (B) but with different characteristic fluctuations; (D) the introduction of a condensing lens to focus light at the sample position resulted in a spectral shift of the fluctuations. These data suggested that the filament emission characteristics and the way in which gratings are illuminated caused significant variations in the recorded spectrum. When diffusers were used, the resulting spectra were smoother and no characteristic fluctuations were present. The diffuser was supposed to reduce spatial variations and polarization effects in the lamp emission. However, the spectra still depended significantly on the type of diffuser placed between the lamp and the objective lens of the spectrograph. The spectra with different configurations mentioned above, after normalization, differed up to 30% in the visible range.

Purcell et al.[79] used the following setup. The light emitted by the calibration lamp passed through a mask and hit a mirror that was tilted with respect to the propagation direction. The mirror had a small central aperture. The light reflected by the mirror illuminated a scattering plate, which diffused radiation back through the small central aperture. This aperture was located at the focus of the collection lens that coupled the light into the spectrograph. The optical path from the lamp to the aperture in the mirror was 0.5 m. This arrangement allowed the authors to image the emission from the entire lamp filament onto the spectrograph slit. The instrument calibration, carried out with the setup above, was validated by measuring the intensity ratio between the 804 and 2855 cm^{-1} bands of cyclohexane at different excitation wavelengths, 458, 488, 514 nm (Ar^+ laser) and 612 nm (dye laser). Without correction, this band ratio varied by almost a factor of four, whereas after applying the instrument calibration, the variation was reduced to about 5%.

5.2. Best Practices for Calibration with Broadband Lamps

According to the previous papers, the following points emerge as the best method for calibrating with a lamp.

- Use of an integrating sphere with the lamp placed inside.

This configuration provides a source of light with uniform radiance at the exit of the sphere, eliminating several issues reported in studies that attempted calibration by directly illuminating the spectrograph entrance slit with the lamp [70]. These issues included non-uniform emission from the lamp filament due to temperature gradients [78] and dependency on the illumination geometry, problem partially mitigated by the use of diffusers [69].

- Reproducing, with the light from the calibration lamp, the same optical pathway as the Raman signal from a real sample.

In this configuration, since the light from the calibration source and the Raman signal from a real sample follow a very similar path from the sample position to the detectors (in particular they illuminate the diffraction grating in the same way), the accuracy of the calibration should be optimal.

- Use of a polarization scrambler before the entrance slit of the spectrograph.

The use of a polarization scrambler before the spectrograph entrance slit is important because, especially the reflectance efficiency of the spectrograph gratings is significantly dependent on light polarization [65]. By depolarizing the incoming radiation, the scrambler minimizes issues arising from differences in the polarization characteristics of the calibration source and the measured samples.

5.3. Advantages and Disadvantages

A first advantage of calibration with the emission of a tungsten–halogen lamp is that it spans a very wide spectral range, typically broad enough to cover the full operating range of most Raman spectrographs. This allows the instrument sensitivity to be determined over the entire accessible range and also to calibrate the anti-Stokes regions. A second advantage is that lamp emission is continuous. This provides a dense set of calibration points, making it possible to correct sharp or periodic features in the IRF: for example, discontinuities introduced when a full spectrum is assembled from multiple segments (segmented acquisition mode) [80], or the etaloning fringes that often appear in back-illuminated CCDs at longer wavelengths [70].

The main disadvantage of lamp-based calibration is the experimental complexity. Proper use of a broadband lamp typically requires an integrating sphere or a carefully designed illumination setup. As a result, this approach is not well suited to routine calibration and is impractical for many laboratories. Another disadvantage is that NIST-traceable calibrated lamps require periodic recalibration; for these lamps, the calibration is typically guaranteed for only about 50 operating hours.

6. Calibration with Luminescent Materials

Fluorescent materials offer a simpler and more practical calibration option than broadband lamps, particularly for routine use. Their emission spectrum can be measured simply by placing them at the sample position, without the need for the more complex setups required by the lamps.

6.1. Standard Reference Materials: Fluorescent Glasses

In the literature, only a few SRMs are reported for the calibration of Raman instruments. Currently, the SRMs available for purchase from NIST are those suitable for calibration at excitation wavelengths of 532 nm (SRM 2242a) [81], 830 nm (SRM 2246a) [82] and 1064 nm (SRM 2244) [83]. The SRM for excitation at 785 nm (SRM 2241) [84] has been released but is not available for purchase at the time of writing, while those for excitation at 488 and 514.5 nm (SRM 2243) [85] and at 633 nm (SRM 2245) [86] have been discontinued. They are glass slides doped with fluorescent inorganic oxides, with sizes 10 × 10 × 1.65 mm or 10.7 × 30.4 × 2 mm. Each SRM is accompanied by a NIST certificate specifying the glass composition, the parameters of the mathematical function describing its emission spectrum, and recommendations regarding its use. They are summarized in Table 2.

It is worth highlighting some relevant points from the calibration procedure of SRMs 2241–2243 [70]:

- The SRMs were rigorously tested against factors that may influence their emission. These included dependence on the instrument configuration (micro- vs. macro-Raman setups, different collection optics, etc.), homogeneity of the glass melt, temperature dependence of the luminescence, and photostability under prolonged laser exposure.

- Polarization effects were mitigated by keeping a polarization scrambler in the setup to ensure that light entering the spectrograph was depolarized both when it came from the SRM and when it came from the real samples.

Table 2. Summary of SRM for calibration of Raman instruments.

NIST Code	Material	λ_{ex} [nm]	Certificate Validity	Availability	Ref.
SRM 2241	Cr_2O_3 doped (0.02% mole fraction) sodium borosilicate matrix glass	785	31/12/2026	Not currently	[84]
SRM 2242a	MnO_2 doped (0.15% weight) borate matrix glass	532	31/12/2029	Yes	[81]
SRM 2243	MnO_2 doped (0.15% weight) borate matrix glass	488, 514.5	01/01/2014	No (discontinued)	[85]
SRM 2244	Cr_2O_3 doped (0.7% mass fraction) borosilicate matrix glass	1064	01/02/2030	Yes	[83]
SRM 2245	Bismuth oxide doped (0.11% mole fraction) in a phosphate matrix glass	633	30/09/2021	No (discontinued)	[86]
SRM 2246a	Chromium oxide doped (0.30% mole fraction) borosilicate glass	830	31/01/2034	Yes	[82]

6.2. Non-Certified Fluorescence Reference Materials

Several commercial fluorescent dyes have their corrected emission spectra reported in the literature, for example in the book by Lakowicz [87]. Although these compounds are not SRMs for Raman spectroscopy, their fluorescence in solution can be used to calibrate the relative spectral response of a Raman spectrometer. Coumarin 540A (also known as Coumarin 153) and quinine sulphate have been studied for this purpose. One Kopp filter glass has also been evaluated with the same aim: this type of materials are commercial optical filter glasses, but certain compositions exhibit measurable fluorescence and have therefore been explored as potential calibration materials. Kopp glasses are still in business, but because years have passed since these evaluations were performed, it is not guaranteed that the current glass formulation is identical to the one originally tested. Table 3 summarizes these materials and the details of the studies that investigated them are reported in the following.

Frost et al. [66] used a calibrated tungsten lamp to determine the true emission spectrum of a 0.84 mM solution of Coumarin 540A in methanol with excitation at 514.5 nm, and the true emission spectrum of Kopp glass 2412, with excitation at 785 nm. Once the emission spectra of these two materials were calibrated, they became secondary standards. Raman spectra of several common organic liquids, including CH_2Cl_2, $CHCl_3$, benzene, acetonitrile and cyclohexane, were measured and corrected using the secondary standard Kopp glass 2412 as a reference. The ratios of selected Raman band areas were compared with those calculated from literature Raman cross sections. The agreement between measured and literature ratios was within 10–20%, which was still quite large but a substantial improvement over the uncorrected spectrum.

Iwata et al. [88] investigated the use of the fluorescence spectrum of quinine (19 mg/L in 1 N H_2SO_4) as an intensity calibration standard for Raman spectrometers. The absolute fluorescence spectrum of quinine, previously reported by Melhuish [89], was fitted with a sixth-order polynomial to obtain a smooth reference function over the visible range. To validate this reference spectrum, the authors measured the rotational Raman spectrum of D_2 gas using 514.5 nm excitation, and, under exactly the same optical configuration, the fluorescence spectrum of the quinine solution, in this case switching the Ar^+ laser to its ultraviolet lines (351.1 or 363.8 nm). The rotational Raman spectrum of D_2 was considered as a primary standard, with known theoretical intensity ratios and was therefore used to derive the IRF by comparing the observed D_2 intensity ratios for some bands with the theoretical values. This IRF was then applied to the measured fluorescence of quinine to work out its true emission spectrum. The resulting calibrated fluorescence spectrum was compared to absolute fluorescence data from Melhuish [89] showing agreement within ±5%.

Table 3. Luminescent reference materials studied for calibration of Raman instruments.

Material	λ_{ex} [nm]	Ref.
Quinine in 1M H_2SO_4	351.1 and 363.8	[88]
Coumarin 153 (540A) in MeOH	514.5	[66]
Kopp glass 2412	785	[66]

6.3. Advantages and Disadvantages

A first advantage of fluorescent materials is that they are extremely easy to use and therefore suitable for routine, day-to-day calibration, even in non-specialized laboratories. Because the emission originates directly at the sample position, the calibration light follows exactly the same optical path as the Raman signal. As discussed in Section 5, this configuration generally ensures a more accurate calibration. Another advantage is that fluorescence spectra are continuous and smooth. Similar to broadband lamps (Section 5.3), they provide a dense set of calibration points, allowing sharp or periodic features in the IRF to be effectively corrected. The availability of SRMs is a major benefit, since their emission properties are rigorously characterized and certified, as described in Section 6.1. Simple reference materials (non-SRMs) provide an alternative to SRMs, although they do not possess the same level of validation.

On the other hand, only a small number of certified fluorescent SRMs exist, and several have been discontinued. Furthermore, each fluorescent standard is valid only for the specific excitation wavelength, whereas broadband lamps can calibrate a much wider spectral range simultaneously. This is a significant limitation, especially considering that diode lasers used in Raman instruments are available at many different wavelengths, in addition to the traditional wavelengths provided by gas lasers. Finally, fluorescent materials cannot be easily used to calibrate the anti-Stokes region.

7. Calibration with Raman Scatterers

Calibration of a Raman spectrometer can also be carried out using Raman spectra themselves. When the relative band intensities of a reference material are known, they can be used to reconstruct the IRF. Although the density of calibration points is lower than when using lamps or fluorescent materials, it can be sufficient to determine the spectral response over the region of interest. Diatomic gases have been used for this purpose, exploiting the fact that certain Raman band cross-section ratios can be accurately calculated from theory. Calibrated Raman spectra of a few organic liquids are available in the literature, although we are not aware of studies where they have been directly used for instrument calibration.

7.1. Diatomic Gases

Raj et al. [39,90] developed a method for the intensity calibration of a Raman instrument that is based on the rotational Raman spectra of H_2, HD, D_2 and vibration-rotation spectra of O_2. The key idea is that the intensity ratio between two rotational Raman bands that originate from the same rotational level is population-independent and can be calculated accurately from theory for these simple molecules. The experimental apparatus consisted of a micro-Raman setup equipped with a 532 nm laser. The samples were a mixture of H_2, HD and D_2, and pure O_2, contained in two separate gas cells. The procedure was as follows.

(1) Initial calibration with a tungsten lamp.

A preliminary calibration step with a tungsten lamp, approximated as a blackbody emitter, was carried out to complement the calibration based on rotational Raman bands, which provides data only at discrete wavenumbers, and to ensure a smooth correction for pixel-to-pixel sensitivity variations.

(2) Acquisition of rotational Raman spectra.

The intensity of a band corresponding to the vibration-rotation transition $v, J \rightarrow v', J \pm 2$ in the diatomic molecules is expressed as:

$$I_{v,J\rightarrow v',J\pm2} = S\left(\tilde{\nu}_{v,J\rightarrow v',J\pm2}\right) I_0 N F_J \, \sigma_{v,J\rightarrow v',J\pm2} \tag{12}$$

$S\left(\tilde{\nu}_{v,J\rightarrow v',J\pm2}\right)$ is the instrument response at the wavenumber at which the vibration-rotation transition $v, J \rightarrow v', J \pm 2$ occurs, I_0 is the laser intensity, N the number of molecules, F_J is the fractional population of rotational state J and $\sigma_{v,J\rightarrow v',J\pm2}$ is the Raman cross section integrated over the collection solid angle. For the transitions $J \rightarrow J+2$ and $J \rightarrow J-2$, which share the same population F_J, their intensity ratio is:

$$\frac{I_{v,J\rightarrow v',J+2}}{I_{v,J\rightarrow v',J-2}} = \frac{\sigma_{v,J\rightarrow v',J+2}}{\sigma_{v,J\rightarrow v',J-2}} \frac{S\left(\tilde{\nu}_{v,J\rightarrow v',J+2}\right)}{S\left(\tilde{\nu}_{v,J\rightarrow v',J-2}\right)} \tag{13}$$

Since the cross-section ratio can be accurately calculated from theory, measurement of the experimental intensity ratio provides the ratio of the instrument responses at the corresponding wavenumbers. Applying this procedure to all accessible bands yielded 13 ratios for the gas mixture (−1034 to 1447 cm^{-1}) and 7 ratios for O_2 (1400 to 1700 cm^{-1}).

To reconstruct the instrument response $S(\tilde{\nu})$, the function was expanded into a power series and the coefficients were obtained by least-squares fitting.

Experiments were performed by placing a polarizer before the entrance slit of the spectrograph, allowing the parallel and perpendicular components of both the Raman spectra and the response function to be measured separately.

(3) Correction of depolarization ratios.

The theoretical depolarization ratio of the Raman bands considered is 0.75, whereas the measured value was about 0.71. The perpendicular component of the instrument response was therefore corrected so that the experimental depolarization ratios matched the theoretical values.

Validation was performed by determining the temperature from Stokes–anti-Stokes ratios, measured in both the parallel and perpendicular polarization configurations, for water and several organic liquids (carbon tetrachloride, cyclohexane, and benzene) and comparing these values with temperatures measured using a thermocouple. The differences relative to the value provided by the thermocouple ranged from 0.4 to 3.2%.

A relevant outcome of this study was the measurement of parallel and perpendicular calibrated Raman spectra of several organic liquids (carbon tetrachloride, cyclohexane, benzene, toluene, and benzonitrile) which can serve as secondary standards for intensity calibration. Depolarization ratios were also calculated for several of their characteristic Raman bands. In this work, the calibration curve extended approximately from −1034 cm^{-1} to 1700 cm^{-1} using 532 nm excitation.

Remarks on Polarization Effects

It is worth noting the different approaches used to control polarization effects when calibrating with fluorescent SRMs (Section 6) and with diatomic gases.

For fluorescent SRMs, a polarization scrambler was placed in front of the spectrograph entrance slit so that the light entering the spectrograph was effectively depolarized either if it came from the SRM or from the actual sample.

For diatomic gases, the opposite approach was used: a polarizer was placed before the entrance slit so that either the parallel or the perpendicular component of the scattered light was selected. The two components were then calibrated independently. Measuring both components yields additional information, but requires twice the number of measurements and is less common in routine Raman spectroscopy.

Experimentally, it is worth highlighting that, besides its undoubted advantage in minimizing polarization effects, the use of a polarization scrambler may pose some experimental issues. Classical quartz-wedge depolarizers introduce a spatially varying retardance that converts the incoming polarization into a mixture of linear, circular, and elliptical states: what is actually achieved is a spatial randomization of the polarization. Their efficiency depends on beam diameter and is typically adequate only for beams larger than ~6 mm; experimental setups must therefore be adapted to accommodate this optic. Liquid-crystal depolarizers, in contrast, can achieve high depolarization efficiency even for small beam diameters. The use of a polarizer (calcite polarizers have very high extinction ratios) is easier to implement.

7.2. Calibrated Raman Spectra of Organic Liquids

Raman spectra of a few organic liquids, with calibrated band ratios, have been published in Ref. [39,48,66] and are summarized in Table 4. Ref. [39] also reported the parallel and perpendicular components of the spectra calibrated separately. Although these liquids could serve as reference materials for Raman intensity calibration, with pros and cons discussed in the next section, to the best of our knowledge there are no reports in which they have actually been used as calibration standards.

Table 4. Organic liquids with calibrated spectra reported in literature. In spectra from Ref. [39] the parallel and perpendicular components are both calibrated.

Liquid	Range [cm^{-1}]	Calibration Sources	λ_{ex} [nm]	Ref.
Acetonitrile	+250 to +3200	Kopp glass 2412	785	[66]
Benzene	−1000 to +1600	Raman vibration-rotation and rotational spectra of diatomic gas molecules	532	[39]
	+250 to +3200	Kopp glass 2412	785	[66]
Benzonitrile	−1000 to +1600	Raman vibration-rotation and rotational spectra of diatomic gas molecules	532	[39]

Table 4. *Cont.*

Liquid	Range [cm^{-1}]	Calibration Sources	λ_{ex} [nm]	Ref.
Carbon tetrachloride	−500 to +1600	Raman vibration-rotation and rotational spectra of diatomic gas molecules	532	[39]
Chloroform	+250 to +3200	Kopp glass 2412	785	[66]
Cyclohexane	−900 to +1600	Raman vibration-rotation and rotational spectra of diatomic gas molecules	532	[39]
	+250 to +3200	Kopp glass 2412	785	[66]
	+400 to +3200	SRM 2242	532	[48]
		SRM 2245	632.8	
		SRM 2241	785	
		SRM 2244	1064	
Dichloromethane	+250 to +3200	Kopp glass 2412	785	[66]
Toluene	−1000 to +1600	Raman vibration-rotation and rotational spectra of diatomic gas molecules	532	[39]

7.3. Advantages and Disadvantages

Since, to the best of our knowledge, organic liquids have not yet been directly employed as intensity calibration standards, the following discussion of their potential advantages and limitations is necessarily speculative.

Similarly to fluorescent materials, organic liquids would be easy to use and suitable for routine calibration. The calibration spectrum would also follow the same optical path as the Raman signal of the actual sample, improving the accuracy of the calibration procedure, as discussed in Sections 5.3 and 6.3. Furthermore, provided that the excitation wavelength lies sufficiently far from any electronic absorption band of the molecule (to avoid resonance effects and self-absorption), a Raman spectrum could in principle be used to calibrate at any excitation wavelength, which would be a significant advantage compared to fluorescent materials. The liquid should exhibit several well-distributed bands spanning a wide spectral range (ideally from ~200 to ~3000 cm^{-1}), with intensities sufficient to ensure a good signal-to-noise ratio. Mixtures could be employed to extend the spectral range or to increase the number of available calibration points. In this case, the relative proportions of the components should be accurately defined. Isolated bands would be ideal; however, overlapping bands, such as those in the C–H stretching region around 3000 cm^{-1}, would not necessarily be a limitation, since they could be treated as a single calibration point by integrating the entire envelope.

On the other hand, calibration points would be present only at the discrete Raman bands of the liquid, limiting the density of reference points. As a result, this approach could fail to capture sharp variations in the IRF, in contrast to broadband lamps or fluorescent materials.

8. Calibration Transfer Methods

In calibration transfer (or model transfer) methods, chemometric procedures are used to adapt a predictive model developed on a primary instrument to a secondary one without physically correcting the instrumental response explicitly: typically, the required mathematical transformation is determined by measuring a set of transfer samples on both instruments [58–62].

Calibration transfer and intensity calibration are not mutually exclusive. Intensity calibration, together with wavenumber and spectral resolution calibration, is expected to strongly reduce spectral variability between instruments. Nevertheless, calibration transfer may still be required to account for two distinct situations: a) residual inter-instrument differences not fully eliminated by the physical calibration; b) changes in sample properties (like variations in physical or chemical composition, temperature, or humidity) that can modify Raman spectral characteristics and invalidate the model even if spectra are all measured in the same instrument (in this case, the procedure is sometimes referred to as calibration maintenance, rather than calibration transfer) [58].

Although most calibration transfer methods were developed and extensively applied in near-infrared spectroscopy, examples of their use in Raman spectroscopy can be found in the literature[91–95].

In the following, we provide a brief conceptual overview of the main approaches used, referring specifically to the transfer between instruments. According to Gemperline [60], these methods can be broadly divided into three categories:

- ***Standardization of predicted values***
- ***Standardization of spectral response***

- ***Methods based on preprocessing techniques***

To fix ideas, let's consider a specific example. A set of n transfer samples is measured on both the primary and the secondary instrument. The spectra are arranged in two matrices, $\boldsymbol{X}_p$ and $\boldsymbol{X}_s$, each of dimensions n x m where n is the number of transfer samples and m is the number of wavenumber points. Each row of $\boldsymbol{X}_p$ and $\boldsymbol{X}_s$ contains the spectrum of one transfer sample measured on the primary and secondary instruments, respectively. The calibration model, developed on the primary instrument, defines a linear relationship between the spectral data and the property of interest (for example the concentration of an analyte):

$$\hat{\boldsymbol{y}}_p = \boldsymbol{X}_p \boldsymbol{b} \tag{14}$$

$\hat{\boldsymbol{y}}_p$ is an n × 1 vector where the *i*-th element is the predicted value for the *i*-th transfer sample measured on the primary instrument, $\boldsymbol{b}$ is an m × 1 vector of model coefficients. For simplicity, no intercept term is included here; if present, it can be accommodated by augmenting $\boldsymbol{X}_p$ with a column of ones and extending $\boldsymbol{b}$ accordingly, without altering the structure of the equations. When the same model is applied to spectra measured on the secondary instrument:

$$\hat{\boldsymbol{y}}_s = \boldsymbol{X}_s \boldsymbol{b} \tag{15}$$

Since the two instruments have different spectral responses, $\hat{\boldsymbol{y}}_s$ will in general differ from $\hat{\boldsymbol{y}}_p$ even for the same samples. This is the problem that calibration transfer aims to solve.

- ***Standardization of predicted values***

In this approach the predicted values are directly corrected. The most common method is the Slope and Bias Correction (SBC) method.

A linear relationship is assumed between the predictions from the primary and secondary instruments, estimated by regressing $\hat{\boldsymbol{y}}_p$ against $\hat{\boldsymbol{y}}_s$ on the transfer samples. The resulting regression coefficients α and β are then used to correct the predictions from the secondary instrument on any new sample:

$$\hat{\boldsymbol{y}}_s(corrected) = \alpha \mathbf{1} + \beta \hat{\boldsymbol{y}}_s \tag{16}$$

This method is simple and robust, and it is most appropriate when the instrumental differences are simple and systematic in all samples measured on the secondary instrument [59,60].

- ***Standardization of spectral response***

Rather than correcting the predicted values, this approach seeks to transform the spectra measured on the secondary instrument so that they resemble those that would have been measured on the primary instrument.

A transformation matrix, $\boldsymbol{F}$, of dimensions m x m, needs to be determined so that:

$$\boldsymbol{X}_p = \boldsymbol{X}_s \boldsymbol{F} \tag{17}$$

Once $\boldsymbol{F}$ is known, any spectrum $\boldsymbol{x}_s^T$ measured in the secondary instrument can be standardized as:

$$\hat{\boldsymbol{x}}_p^T = \boldsymbol{x}_s^T \boldsymbol{F} \tag{18}$$

and then used directly with the original model coefficients $\boldsymbol{b}$ to obtain a corrected prediction. The superscript T indicates the transpose. $\boldsymbol{F}$ can be estimated by several methods. In Direct Standardization (DS), $\boldsymbol{F}$ is computed using the pseudo-inverse (indicated with +) of the secondary spectra matrix:

$$\boldsymbol{F} = \boldsymbol{X}_s^+ \boldsymbol{X}_p \tag{19}$$

In this formulation, each wavenumber channel in the standardized spectrum is reconstructed as a linear combination of all wavenumber channels of the secondary instrument. The main limitation of DS is that the number of transfer samples n is typically much smaller than the number of spectral points m, which may lead to ill-conditioned estimation problems. A more common approach is Piecewise Direct Standardization (PDS), in which each wavenumber channel of the standardized spectrum is correlated only to a small window of neighboring wavenumber channels of the secondary instrument. Mathematically, the transformation matrix takes a block-diagonal banded form, rather than the full dense form of DS, which greatly reduces the number of parameters to be estimated and improves numerical stability. Other methods have also been proposed; the reader is referred to the literature for details [59,60].

- ***Preprocessing-based methods***

In preprocessing-based calibration transfer, the same spectral procedures are applied independently to spectra acquired on different instruments, in order to reduce systematic differences before model application.

Since these corrections do not require transfer samples measured on both instruments, they are particularly convenient when such samples are not available. These methods are most effective when the spectra from different instruments differ in a simple, uniform way across the entire spectral range. For example, one instrument may systematically record higher intensities than another by a constant factor (multiplicative effect), because of different laser power, penetration depth in the sample etc. Alternatively, the baseline of one instrument may be shifted by a constant amount relative to another (additive effect), because of fluorescence background for example. In these cases, a simple rescaling and/or offset correction is sufficient to bring the spectra into agreement. Typical preprocessing methods include baseline correction, spectral derivatives (the first derivative removes constant offsets, while the second derivative additionally removes linear trends) and Multiplicative Scatter Correction (MSC). MSC assumes that each spectrum differs from a reference spectrum (usually the mean of the dataset) by an additive offset and a multiplicative scaling factor. These parameters are estimated by regression and subsequently used to correct the spectrum itself. A related method, Standard Normal Variate (SNV), achieves a similar correction without requiring a reference spectrum, by standardizing each spectrum using its own mean and standard deviation [59,60].

9. Interlaboratory Comparison

Interlaboratory studies have been recently reviewed by Rusu et al. [96]. Here, we discuss two representative studies that explicitly addressed intensity calibration procedures and the comparability of Raman instruments.

Guo et al. [97] conducted a round-robin experiment involving 35 Raman setups from 15 laboratories, within the COST action Raman4clinics, that was specifically designed to quantify the variability of Raman spectra across different instrumentation. The participating instruments spanned a wide variety of optical designs, including highly confocal microscopes and fiber-optic systems, operating at 514.5 nm, 532 nm, and 785 nm excitation wavelengths. Cyclohexane has known integrated-intensity band ratios, and it was used to assess intensity variations across different instruments. Representative findings, relevant to the intensity calibration are the following:

- The areas of the cyclohexane bands at 1028, 1266, and 1444 cm^{-1} were integrated and normalized to the 801 cm^{-1} band. The observed ratios varied widely among different instruments, $\frac{A(1028\ cm^{-1})}{A(801\ cm^{-1})} = 0.45 - 0.70$, $\frac{\mathrm{A}(1266\ \mathrm{cm}^{-1})}{\mathrm{A}(801\ \mathrm{cm}^{-1})} = 0.35 - 0.65$, $\frac{\mathrm{A}(1444\ \mathrm{cm}^{-1})}{\mathrm{A}(801\ \mathrm{cm}^{-1})} = 0.35 - 0.75$. Even within the limited spectral window 801–1444 cm^{-1} the relative intensities varied by up to a factor of two. Larger discrepancies are expected when including bands near 3000 cm^{-1}, where the C–H and O–H stretching modes fall. Figure 6 summarizes the results from all participants.
- A manufacturer built-in intensity calibration was applied in four instruments. However, this procedure did not improve inter-instrument agreement. As illustrated by the arrows in Figure 6, the correction shifts the ratios, but does not produce a clear reduction in variability after calibration. These findings were interpreted by the authors as inaccuracy of the estimated IRF.

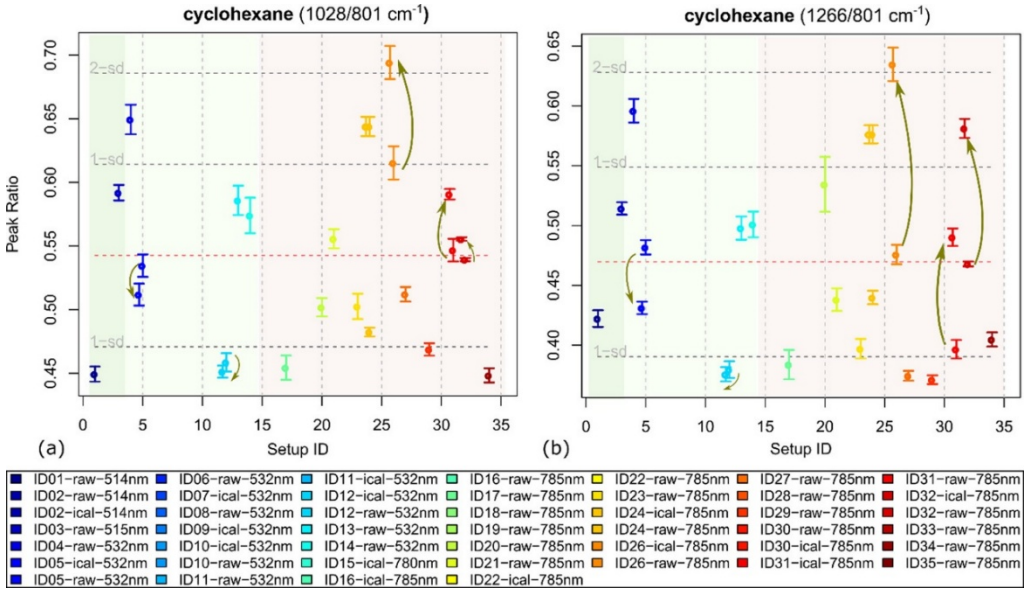

Figure 6. Peak area of the 1028 (**a**) and 1266 cm^{-1} (**b**) bands of cyclohexane normalized to the 801 cm^{-1} one. Each ID corresponds to a participating laboratory. "Raw" denotes data acquired without intensity calibration, while "ical"

indicates that an intensity calibration was applied. Background colors indicate different excitation wavelengths. Arrows show how the measured ratio changes after applying the laboratory intensity calibration. Reproduced with permission from Ref. [97].

Turner et al. [98] performed an international interlaboratory comparison involving 17 participants from 13 countries, under the Versailles Project on Advanced Materials and Standards (VAMAS). The setup used either 514.5 or 532 nm excitation wavelength and most of them used a 100× in a micro-Raman instrument. A single, large CVD-grown graphene film was prepared by the lead participant (NPL), transferred onto Si/SiO_2 (300 nm), cut into 10 × 10 mm samples, and distributed. Each laboratory measured two locations on the sample: one near the edge and one near the center of the graphene sheet. At each location, a 10 × 10 μm Raman map (121 spectra) was acquired, following a common protocol. The 121 spectra were then averaged to obtain the Raman metrics for that area. The authors examined the I_{2D}/I_G intensity ratio, with the G band located at ~1580 cm^{-1} and the 2D band located at ~2700 cm^{-1}: this ratio, in combination with other parameters, can be used as an indicator of the graphene layer number (monolayer graphene typically exhibits $I_{2D}/I_G \geq 2$). Representative findings from this paper, in the context of intensity calibration, are the following:

- Reported I_{2D}/I_G values ranged from ~1 to 4; one participant, whose spectrometer was optimized for infrared excitation, reported a value close to 6. Differences arising from data analysis were shown to be negligible, and sample heterogeneity (wrinkles, folds) may have contributed to some extent, but the spread was attributed mainly to instrumental factors.
- Three participants performed intensity calibration of their spectrometers: the lead participant, using NIST SRM 2242a, and participants #6 and #14, both using a broadband lamp. It is worth making a restricted comparison among these participants: the lead participant remeasured the same samples that were sent to #6 and #14, nominally in the same regions. It was verified that the maps measured by the lead and #6 were very consistent, making this comparison particularly meaningful: the comparison of the I_{2D}/I_G values showed an almost perfect agreement between the lead and #6, with a relative difference of 0.4% in the edge area, the lowest observed among all participants. In the center area, however, the relative difference was 25%: the authors attributed this discrepancy to the fact that in the central area, the 2D peak is larger and more difficult to fit, possibly producing differences in the estimated areas. The relative differences between the lead and #14 were ~7% in the edge and ~18% in the center.
- Table 5 summarizes the I_{2D}/I_G values before and after calibration. Data are extracted from the supporting info and show how much the calibration procedure impacts the values of the ratios. It increased by 10% for the lead participant and by 25% for participant #6, confirming the rather strong impact.

Table 5. I_{2D}/I_G values measured by the lead participant and by partecipant #6, with and without intensity calibration. The data from the lead participant are the average of all samples sent to participants and over edge and center regions. Data extracted from the supporting information of Ref. [98].

	I_{2D}/I_G		
	Lead	**#6 (Edge)**	**#6 (center)**
After calibration	2.2	1.27	1.94
Before calibration	2.0	1.02	1.55

Overall, these interlaboratory studies showed that instrument-to-instrument variations were substantial, up to a factor of 2 in the band ratio of selected cyclohexane peaks [97] and up to a factor of 4–6 when the I_{2D}/I_G ratio was evaluated for graphene [98]. Such variations are too large for applications in which the ratio has intrinsic physical meaning, as in graphene, where I_{2D}/I_G is linked, along with other parameters, to the number of layers: if the reference value of 2 is used to distinguish monolayer from multilayer graphene, but the measured values range from 1 to 4, the metric becomes unusable. Similarly, these variations are too large for reliable compound recognition based on band ratios.

The use of calibrated spectra was quite limited, as most laboratories collected data without any intensity calibration. In the case of Guo et al. [97], the calibration procedure relied on instrument built-in routines, for which no details were available. This lack of information made it difficult to ensure that the same procedure was applied across laboratories.

Both studies strongly support the conclusion that intensity calibration is essential for improving the comparability of spectra acquired on different instruments.

10. Selection of the Intensity Calibration Method

The most appropriate strategy for intensity calibration depends on several factors, like the type of measurements, the type of instrumentation available, and the level of spectroscopic expertise of the operator. The following examples tentatively illustrate typical laboratory situations in which different calibration approaches may be preferred. Note that additional considerations, such as cost and recalibration frequency, also affect the choice of calibration method and are intertwined with the scenarios described above; they are briefly discussed at the end of this section.

- ***Laboratories with configurable instruments and good spectroscopic expertise.*** In this case, broadband lamps are probably the best choice. They allow the calibration of the entire spectral range of the instrument, very useful for example when several excitation wavelengths are available or when both Stokes and anti-Stokes spectra are needed. The main drawback is that their use typically requires good expertise and modification of the optical setup to accommodate the light source. NIST SRMs represent a valid alternative in this context when experimental simplicity is preferred over full spectral coverage. The use of other methods, non-certified fluorescence materials or Raman scatterers, is of course also possible, in case of specific experimental requirements.
- ***Laboratories where Raman spectroscopy is mainly employed as a routine analytical technique using non configurable instruments.*** In this case, calibration procedures must be easy to implement: NIST SRMs represent the most practical solution. When SRMs are not available, non-certified fluorophores or organic liquids can serve as alternative reference standards. Although their spectra reported in the literature are not officially certified by a metrological institute, they can still be useful for improving inter-instrument comparability. Since no official procedures exist for these materials, the calibration protocol must be established by the laboratory itself, based on the procedures reported in the literature.
- ***Laboratories that require a high level of regulation and standardization****,* like in the pharmaceutical field. In this case, NIST SRMs are the most appropriate choice. Moreover, their ease of use makes them suitable for periodic verification of the instrument calibration.

Cost considerations. NIST-calibrated broadband lamps mounted in an integrating sphere require a significant initial investment, on the order of several thousands of euros, and their calibration is typically guaranteed for only about 50 operating hours. NIST SRMs are also quite expensive, with a price on the order of two thousand euros per slide. Their validity period, specified in the accompanying certificate, can extend to several years, as summarized in Table 2. Non-certified fluorophores and organic liquids are inexpensive and readily available, making them attractive options when budget is a constraint.

Recalibration frequency. NIST SRMs are the most suitable options for routine periodic verification. Broadband lamps, on the other hand, are better suited for non-routine calibration, like the initial characterization of a new instrument or after significant optical modifications, given the greater experimental complexity they involve. It is also possible to adopt a hybrid strategy, in which an initial calibration over the full spectral range is performed using a broadband lamp, while rapid periodic verification of the instrument response is carried out using SRMs (or in case non-certified fluorophores).

Finally, Table 6 summarizes the advantages and disadvantages of the calibration strategies discussed in the previous sections of this review, together with their suggested typical application scenarios.

Table 6. Summary of advantages and disadvantages of the different calibration methods and their suggested typical application scenarios. ✓ and ✗ indicate whether the criterion is met or not, respectively. (*) Organic liquids have been only proposed as Raman calibration materials; therefore, their criteria are included here on a hypothetical basis. (**) This refers to the best configuration, in which the output from the integrating sphere is let through the microscope objective mimicking light emitted from the sample.

Criterion	Broadband Lamps	Fluorescence Materials		Raman Scatterers	
		NIST SRM	Non-Certified Fluorophores	Diatomic Gases	Organic Liquids (*)
Ease of use	✗	✓	✓	✗	✓
SRM	✗	✓	✗	✗	✗
Usable at multiple λ_{ex}	✓	✗	✗	✓	✓
Matches sample optical path	✓ (**)	✓	✓	✓	✓
Dense calibration points	✓	✓	✓	✗	✗
Anti-Stokes calibration possible	✓	✗	✗	✓	✓
Low cost	✗	✗	✓	✗	✓

Table 6. *Cont.*

Criterion	Broadband Lamps	Fluorescence Materials		Raman Scatterers	
		NIST SRM	Non-Certified Fluorophores	Diatomic Gases	Organic Liquids (*)
Typical application scenario					
Labs with configurable instruments and good spectroscopic expertise.	✓	✓	✓	✓	✓
Labs where Raman spectroscopy is mainly employed as a routine analytical technique using non-configurable instruments.	✗	✓	✓	✗	✓
Labs that require a high level of regulation and standardization	✗	✓	✗	✗	✗

11. Concluding Remarks

Despite the widespread use of Raman spectroscopy across scientific and technological domains, the calibration of Raman intensities remains insufficiently adopted. The interlaboratory studies examined here clearly demonstrate that relative band intensities vary significantly from one instrument to another, often by more than a factor of two. For applications in which intensity ratios reflect fundamental physical or chemical properties, such discrepancies limit the reliability of quantitative analyses. More broadly, inter-instrument variability in spectral response complicates the development of unified spectral databases and hinders the inter-instrument transferability of chemometric and machine learning models, two areas of growing importance as Raman spectroscopy becomes increasingly integrated with data-driven approaches.

Methods suitable for routine intensity calibration are currently constrained by the limited availability of appropriate reference materials. NIST Standard Reference Materials remain the gold standard, offering the highest level of validation and traceability, but they do not cover all excitation wavelengths and several have been discontinued. This situation highlights the need to expand the range of validated reference materials, both certified and non-certified. One possible direction in this regard is the further investigation of organic liquids as calibration standards. Their key advantage lies in the fact that a single liquid can in principle support calibration at multiple excitation wavelengths. The limited density of calibration points could be partially mitigated through the use of mixtures.

Physical intensity calibration and calibration transfer methods are complementary strategies for achieving inter-instrument comparability. Since residual differences may persist even after physical calibration, combining the two approaches is expected to yield better overall results.

Author Contributions

The author confirms being the sole contributor of this work and has approved it for publication.

Funding

This research received no external funding.

Institutional Review Board Statement

Not applicable.

Informed Consent Statement

Not applicable.

Data Availability Statement

No new data were created in this study. Data sharing is not applicable to this article.

Conflicts of Interest

The author declares no conflict of interest.

Use of AI and AI-Assisted Technologies

During the preparation of this work, the author used ChatGPT (OpenAI) to revise English. After using this tool, the author reviewed and edited the content as needed and takes full responsibility for the content of the published article.

References

1. Smith, E.; Dent, G. *Modern Raman Spectroscopy: A Practical Approach*; John Wiley & Sons, Inc.: Chichester, UK, 2005; ISBN 0-471-49668-5.
2. *Handbook of Raman Spectroscopy: From the Research Laboratory to the Process Line*; Lewis, I.R., Edwards, H.G.M., Eds.; Practical Spectroscopy; CRC Press: New York, NY, USA, 2001; Volume 28; ISBN 978-0-8247-0557-2.
3. Esmonde-White, K.A.; Cuellar, M.; Uerpmann, C.; et al. Raman Spectroscopy as a Process Analytical Technology for Pharmaceutical Manufacturing and Bioprocessing. *Anal. Bioanal. Chem.* **2017**, *409*, 637–649. https://doi.org/10.1007/s00216-016-9824-1.
4. Vankeirsbilck, T.; Vercauteren, A.; Baeyens, W.; et al. Applications of Raman Spectroscopy in Pharmaceutical Analysis. *TrAC Trends Anal. Chem.* **2002**, *21*, 869–877. https://doi.org/10.1016/S0165-9936(02)01208-6.
5. Eshbekova, N.; Sowndarya, A.; Thangadurai, T.D.; et al. Recent Advancements in Raman Instrumentation and Capabilities for Pharmaceutical and Biomedical Applications. *Appl. Spectrosc. Rev.* **2024**, *59*, 798–849. https://doi.org/10.1080/05704928.2024.2355193.
6. Laplant, F.; De Paepe, A. Raman Spectroscopy for Identifying Polymorphs. In *Pharmaceutical Applications of Raman Spectroscopy*; Šašić, S., Ed.; John Wiley & Sons, Ltd.: Hoboken, NJ, USA, 2007; pp. 85–115. ISBN 978-0-470-22588-2.
7. Cong, X.; Liu, X.L.; Lin, M.L.; et al. Application of Raman Spectroscopy to Probe Fundamental Properties of Two-Dimensional Materials. *2D Mater. Appl.* **2020**, *4*, 1–12. https://doi.org/10.1038/s41699-020-0140-4.
8. Jorio, A.; Saito, R.; Dresselhaus, G.; et al. *Raman Spectroscopy in Graphene Related Systems*; Wiley-VCH Verlag GmbH & Co. KGaA: Weinheim, Germany, 2011; ISBN 978-3-527-40811-5.
9. Castiglioni, C.; Mapelli, C.; Negri, F.; et al. Origin of the D Line in the Raman Spectrum of Graphite: A Study Based on Raman Frequencies and Intensities of Polycyclic Aromatic Hydrocarbon Molecules. *J. Chem. Phys.* **2001**, *114*, 963–974. https://doi.org/10.1063/1.1329670.
10. Ferrari, A.C.; Robertson, J. Interpretation of Raman Spectra of Disordered and Amorphous Carbon. *Phys. Rev. B* **2000**, *61*, 14095–14107. https://doi.org/10.1103/PhysRevB.61.14095.
11. *Vibrational Spectroscopy of Polymers. Principles and Practises*; Everall, N.J., Chalmers, J.M., Griffiths, P.R., Eds.; John Wiley & Sons, Ltd.: Chichester, UK, 2007; ISBN 978-0-470-01662-6.
12. *Modern Polymer Spectroscopy*; Zerbi, G., Ed.; Wiley-VCH Verlag GmbH: New York, NY, USA, 2008; ISBN 978-3-527-61393-9.
13. Castiglioni, C.; Tommasini, M.; Zerbi, G. Raman Spectroscopy of Polyconjugated Molecules and Materials: Confinement Effect in One and Two Dimensions. *Philos. Trans. R. Soc. Math. Phys. Eng. Sci.* **2004**, *362*, 2425–2459. https://doi.org/10.1098/RSTA.2004.1448.
14. Caggiani, M.C.; Colomban, P. Advanced Procedures in Raman Forensic, Natural, and Cultural Heritage Studies: Mobile Set-up, Optics, and Data Treatment—State of the Art and Perspectives. *J. Raman Spectrosc.* **2024**, *55*, 116–124. https://doi.org/10.1002/JRS.6633.
15. Rousaki, A.; Vandenabeele, P. In Situ Raman Spectroscopy for Cultural Heritage Studies. *J. Raman Spectrosc.* **2021**, *52*, 2178–2189. https://doi.org/10.1002/JRS.6166.
16. Froment, F.; Tournié, A.; Colomban, P. Raman Identification of Natural Red to Yellow Pigments: Ochre and Iron-Containing Ores. *J. Raman Spectrosc.* **2008**, *39*, 560–568. https://doi.org/10.1002/JRS.1858.
17. Angelini, I.; Asscher, Y.; Secco, M.; et al. The Pigments of the Frigidarium in the Sarno Baths, Pompeii: Identification, Stratigraphy and Weathering. *J. Cult. Herit.* **2019**, *40*, 309–316. https://doi.org/10.1016/J.CULHER.2019.04.021.
18. Vandenabeele, P.; Edwards, H.G.M.; Jehlička, J. The Role of Mobile Instrumentation in Novel Applications of Raman Spectroscopy: Archaeometry, Geosciences, and Forensics. *Chem. Soc. Rev.* **2014**, *43*, 2628–2649. https://doi.org/10.1039/C3CS60263J.
19. Rull, F.; Maurice, S.; Hutchinson, I.; et al. The Raman Laser Spectrometer for the ExoMars Rover Mission to Mars. *Astrobiology* **2017**, *17*, 627–654. https://doi.org/10.1089/AST.2016.1567.
20. LeRu, E.C.; Etchegoin, P.G. *Principles of Surface Enhanced Raman Spectroscopy*; Elsevier: Amsterdam, The Netherlands, 2009; ISBN 978-0-444-52779-0.
21. Pilot, R.; Signorini, R.; Fabris, L. Surface-Enhanced Raman Spectroscopy: Principles, Substrates, and Applications. In *Metal Nanoparticles and Clusters: Advances in Synthesis, Properties and Applications*; Deepak, F.L., Ed.; Springer: Berlin, Germany, 2017; pp. 89–164. ISBN 978-3-319-68052-1.

22. Pilot, R.; Signorini, R.; Durante, C.; et al. A Review on Surface-Enhanced Raman Scattering. *Biosensors* **2019**, *9*, 57. https://doi.org/10.3390/bios9020057.
23. Yi, J.; You, E.M.; Hu, R.; et al. Surface-Enhanced Raman Spectroscopy: A Half-Century Historical Perspective. *Chem. Soc. Rev.* **2025**, *54*, 1453–1551. https://doi.org/10.1039/D4CS00883A.
24. Langer, J.; Aberasturi, D.J. de; Aizpurua, J.; et al. Present and Future of Surface-Enhanced Raman Scattering. *ACS Nano* **2019**, *14*, 28–117. https://doi.org/10.1021/acsnano.9b04224.
25. Bell, S.E.J.; Charron, G.; Cortés, E.; et al. Towards Reliable and Quantitative Surface-Enhanced Raman Scattering (SERS): From Key Parameters to Good Analytical Practice. *Angew. Chem. Int. Ed.* **2020**, *59*, 5454–5462. https://doi.org/10.1002/ANIE.201908154.
26. Bodelón, G.; Pastoriza-Santos, I. Recent Progress in Surface-Enhanced Raman Scattering for the Detection of Chemical Contaminants in Water. *Front. Chem.* **2020**, *8*, 518752. https://doi.org/10.3389/fchem.2020.00478.
27. Ong, T.T.X.; Blanch, E.W.; Jones, O.A.H. Surface Enhanced Raman Spectroscopy in Environmental Analysis, Monitoring and Assessment. *Sci. Total Environ.* **2020**, *720*, 137601. https://doi.org/10.1016/J.SCITOTENV.2020.137601.
28. Zheng, J.; He, L. Surface-Enhanced Raman Spectroscopy for the Chemical Analysis of Food. *Compr. Rev. Food Sci. Food Saf.* **2014**, *13*, 317–328. https://doi.org/10.1111/1541-4337.12062.
29. Cialla-May, D.; Bonifacio, A.; Bocklitz, T.; et al. Biomedical SERS—The Current State and Future Trends. *Chem. Soc. Rev.* **2024**, *53*, 8957–8979. https://doi.org/10.1039/D4CS00090K.
30. Fornasaro, S.; Cialla-May, D.; Sergo, V.; et al. The Role of Surface Enhanced Raman Scattering for Therapeutic Drug Monitoring of Antimicrobial Agents. *Chemosensors* **2022**, *10*, 128. https://doi.org/10.3390/CHEMOSENSORS10040128.
31. Chisanga, M.; Muhamadali, H.; Ellis, D.I.; et al. Surface-Enhanced Raman Scattering (SERS) in Microbiology: Illumination and Enhancement of the Microbial World. *Appl. Spectrosc.* **2018**, *72*, 987–1000. https://doi.org/10.1177/0003702818764672.
32. Stefancu, A.; Aizpurua, J.; Alessandri, I.; et al. Impact of Surface Enhanced Raman Spectroscopy in Catalysis. *ACS Nano* **2024**, *18*, 29337–29379. https://doi.org/10.1021/acsnano.4c06192.
33. Pozzi, F.; Leona, M. Surface-Enhanced Raman Spectroscopy in Art and Archaeology. *J. Raman Spectrosc.* **2016**, *47*, 67–77. https://doi.org/10.1002/JRS.4827.
34. Nicolson, F.; Kircher, M.F.; Stone, N.; et al. Spatially Offset Raman Spectroscopy for Biomedical Applications. *Chem. Soc. Rev.* **2021**, *50*, 556–568. https://doi.org/10.1039/D0CS00855A.
35. Matousek, P. Spatially Offset Raman Spectroscopy for Non-Invasive Analysis of Turbid Samples. *TrAC Trends Anal. Chem.* **2018**, *103*, 209–214. https://doi.org/10.1016/J.TRAC.2018.04.002.
36. Eliasson, C.; Matousek, P. Noninvasive Authentication of Pharmaceutical Products through Packaging Using Spatially Offset Raman Spectroscopy. *Anal. Chem.* **2007**, *79*, 1696–1701. https://doi.org/10.1021/ac062223z.
37. Eliasson, C.; Macleod, N.A.; Matousek, P. Noninvasive Detection of Concealed Liquid Explosives Using Raman Spectroscopy. *Anal. Chem.* **2007**, *79*, 8185–8189. https://doi.org/10.1021/ac071383n.
38. McCreery, R.L. *Raman Spectroscopy for Chemical Analysis*; Winefordner, J.D., Ed.; Chemical Analysis; John Wiley & Sons, Inc.: Hoboken, NJ, USA, 2000; Volume 157; ISBN 978-0-471-25287-0.
39. Raj, A.; Kato, C.; Witek, H.A.; et al. Toward Standardization of Raman Spectroscopy: Accurate Wavenumber and Intensity Calibration Using Rotational Raman Spectra of H_2, HD, D_2, and Vibration–Rotation Spectrum of O_2. *J. Raman Spectrosc.* **2020**, *51*, 2066–2082. https://doi.org/10.1002/jrs.5955.
40. Itoh, N.; Shirono, K. Reliable Estimation of Raman Shift and Its Uncertainty for a Non-Doped Si Substrate (NMIJ CRM 5606-a). *J. Raman Spectrosc.* **2020**, *51*, 2496–2504. https://doi.org/10.1002/JRS.6003.
41. *Standard Guide for Raman Shift Standards for Spectrometer Calibration*; ASTM International: West Conshohocken, PA, USA, 2014.
42. *Standard Guide for Testing the Resolution of a Raman Spectrometer*; ASTM International: West Conshohocken, PA, USA, 2022.
43. Jakubek, R.S.; Fries, M.D. Calibration of the Temporal Drift in Absolute and Relative Raman Intensities in Large Raman Images Using a Mercury–Argon Lamp. *J. Raman Spectrosc.* **2022**, *53*, 137–147. https://doi.org/10.1002/JRS.6259.
44. Jakubek, R.S.; Fries, M.D. Calibration of Raman Wavenumber in Large Raman Images Using a Mercury-Argon Lamp. *J. Raman Spectrosc.* **2020**, *51*, 1172–1185. https://doi.org/10.1002/JRS.5887.
45. Jakubek, R.S.; Fries, M.D. Raman Instrument Calibration for Astromaterials and Analysis of Mars Return Samples. *Meteorit. Planet. Sci.* **2023**, *58*, 98–110. https://doi.org/10.1111/maps.13940.
46. Gou, L.; Zeng, X.; Du, H.; et al. Sensitive Detection of Trace 4-Methylimidazole Utilizing a Derivatization Reaction-Based Ratiometric Surface-Enhanced Raman Scattering Platform. *Talanta* **2022**, *237*, 122925. https://doi.org/10.1016/j.talanta.2021.122925.

47. Li, L.; Zhang, L.; Gou, L.; et al. Au Nanoparticles Decorated CoP Nanowire Array: A Highly Sensitive, Anticorrosive, and Recyclable Surface-Enhanced Raman Scattering Substrate. *Anal. Chem.* **2023**, *95*, 11037–11046. https://doi.org/10.1021/acs.analchem.3c01282.
48. *Standard Guide for Relative Intensity Correction of Raman Spectrometers*; ASTM International: West Conshohocken, PA, USA, 2023.
49. Lussier, F.; Thibault, V.; Charron, B.; et al. Deep Learning and Artificial Intelligence Methods for Raman and Surface-Enhanced Raman Scattering. *TrAC Trends Anal. Chem.* **2020**, *124*, 115796. https://doi.org/10.1016/J.TRAC.2019.115796.
50. Guo, S.; Popp, J.; Bocklitz, T. Chemometric Analysis in Raman Spectroscopy from Experimental Design to Machine Learning–Based Modeling. *Nat. Protoc.* **2021**, *16*, 5426–5429. https://doi.org/10.1038/s41596-021-00620-3.
51. Blake, N.; Gaifulina, R.; Griffin, L.D.; et al. Machine Learning of Raman Spectroscopy Data for Classifying Cancers: A Review of the Recent Literature. *Diagnostics* **2022**, *12*, 1491. https://doi.org/10.3390/diagnostics12061491.
52. Coca-Lopez, N.; Alcolea-Rodriguez, V.; Ares, M.A.B.; et al. Artificial Intelligence-Powered Raman Spectroscopy through Open Science and FAIR Principles. *ACS Nano* **2025**, *19*, 38189–38218. https://doi.org/10.1021/ACSNANO.5C09165.
53. Yang, Y.; Xu, B.; Murray, J.; et al. Rapid and Quantitative Detection of Respiratory Viruses Using Surface-Enhanced Raman Spectroscopy and Machine Learning. *Biosens. Bioelectron.* **2022**, *217*, 114721. https://doi.org/10.1016/J.BIOS.2022.114721.
54. Botto, C.S.; Orecchio, C.; D'Errico, C.; et al. Rapid Classification of Bacteria by a Portable Raman Spectrometer and Machine Learning. *Spectrochim. Acta. A. Mol. Biomol. Spectrosc.* **2026**, *344*, 126701. https://doi.org/10.1016/J.SAA.2025.126701.
55. Zhang, L.; Li, C.; Peng, D.; et al. Raman Spectroscopy and Machine Learning for the Classification of Breast Cancers. *Spectrochim. Acta. A. Mol. Biomol. Spectrosc.* **2022**, *264*, 120300. https://doi.org/10.1016/J.SAA.2021.120300.
56. Bocklitz, T.W.; Dörfer, T.; Heinke, R.; et al. Spectrometer Calibration Protocol for Raman Spectra Recorded with Different Excitation Wavelengths. *Spectrochim. Acta. A. Mol. Biomol. Spectrosc.* **2015**, *149*, 544–549. https://doi.org/10.1016/j.saa.2015.04.079.
57. Georgiev, G.; Coca-Lopez, N.; Lellinger, D.; et al. Open Source for Raman Spectroscopy Data Harmonization. *J. Raman Spectrosc.* **2025**, *56*, 878–881. https://doi.org/10.1002/jrs.6789.
58. Workman, J.J. A Review of Calibration Transfer Practices and Instrument Differences in Spectroscopy. *Appl. Spectrosc.* **2018**, *72*, 340–365. https://doi.org/10.1177/0003702817736064.
59. Feudale, R.N.; Woody, N.A.; Tan, H.; et al. Transfer of Multivariate Calibration Models: A Review. *Chemom. Intell. Lab. Syst.* **2002**, *64*, 181–192. https://doi.org/10.1016/S0169-7439(02)00085-0.
60. *Practical Guide to Chemometrics*, 2nd ed.; Gemperline, P., Ed.; CRC Press: Boca Raton, FL, USA, 2006; ISBN 978-0-429-11956-9.
61. Ramadan, A.; Robert, G.; Kersaudy, R.; et al. Calibration Transfer and Maintenance in the Pharmaceutical Industry: A Systematic Review. *Eur. J. Pharm. Sci.* **2025**, *209*, 107114. https://doi.org/10.1016/j.ejps.2025.107114.
62. Barton, B.; Thomson, J.; Lozano Diz, E.; et al. Chemometrics for Raman Spectroscopy Harmonization. *Appl. Spectrosc.* **2022**, *76*, 1021–1041. https://doi.org/10.1177/00037028221094070.
63. Ntziouni, A.; Thomson, J.; Xiarchos, I.; et al. Review of Existing Standards, Guides, and Practices for Raman Spectroscopy. *Appl. Spectrosc.* **2022**, *76*, 747–772. https://doi.org/10.1177/00037028221090988.
64. Guo, S.; Popp, J.; Bocklitz, T. Key Steps in the Workflow to Analyze Raman Spectra. *Spectroscopy* **2023**, *38*, 30–33. https://doi.org/10.56530/spectroscopy.fl6984w5.
65. Adar, F. Raman Polarization Measurements: Keeping Track of the Instrumental Components' Behavior. *Spectroscopy* **2017**, *32*, 14–22.
66. Frost, K.J.; McCreery, R.L. Calibration of Raman Spectrometer Instrument Response Function with Luminescence Standards: An Update. *Appl. Spectrosc.* **1998**, *52*, 1614–1618.
67. Tuschel, D. Spectral Resolution and Dispersion in Raman Spectroscopy. *Spectroscopy* **2020**, *35*, 9–15.
68. Mooney, J.; Kambhampati, P. Get the Basics Right: Jacobian Conversion of Wavelength and Energy Scales for Quantitative Analysis of Emission Spectra. *J. Phys. Chem. Lett.* **2013**, *4*, 3316–3318. https://doi.org/10.1021/jz401508t.
69. Malyj, M.; Griffiths, J.E. Stokes/Anti-Stokes Raman Vibrational Temperatures: Reference Materials, Standard Lamps, and Spectrophotometric Calibrations. *Appl. Spectrosc.* **1983**, *37*, 315–333. https://doi.org/10.1366/0003702834634325.
70. Choquette, S.J.; Etz, E.S.; Hurst, W.S.; et al. Relative Intensity Correction of Raman Spectrometers: NIST SRMs 2241 through 2243 for 785 nm, 532 nm, and 488 nm/514.5 nm Excitation. *Appl. Spectrosc.* **2007**, *61*, 117–129. https://doi.org/10.1366/000370207779947585.
71. Ying, X. An Overview of Overfitting and Its Solutions. *J. Phys. Conf. Ser.* **2019**, *1168*, 022022. https://doi.org/10.1088/1742-6596/1168/2/022022.
72. Fang, S.; Wu, S.; Chen, Z.; et al. Recent Progress and Applications of Raman Spectrum Denoising Algorithms in Chemical and Biological Analyses: A Review. *TrAC Trends Anal. Chem.* **2024**, *172*, 117578. https://doi.org/10.1016/j.trac.2024.117578.
73. Palchetti, L.; Bianchini, G.; Castagnoli, F. Design and Characterisation of Black-Body Sources for Infrared Wide-Band Fourier Transform Spectroscopy. *Infrared Phys. Technol.* **2008**, *51*, 207–215. https://doi.org/10.1016/J.INFRARED.2007.06.001.

74. Petty, C.J.; Warnes, G.M.; Hendra, P.J.; et al. Relative Intensity Calibration of Single-Beam near-Infrared Spectrometers. *Spectrochim. Acta Part Mol. Spectrosc.* **1991**, *47*, 1179–1187. https://doi.org/10.1016/0584-8539(91)80205-W.
75. Georgiev, G.T.; Butler, J.J. Long-Term Calibration Monitoring of Spectralon Diffusers BRDF in the Air-Ultraviolet. *Appl. Opt.* **2007**, *46*, 7892–7899. https://doi.org/10.1364/AO.46.007892.
76. Hapke, B. *Theory of Reflectance and Emittance Spectroscopy*; 2nd ed.; Cambridge University Press: Cambridge, UK, 2012; ISBN 978-0-521-88349-8.
77. Fryling, M.; Frank, C.J.; McCreery, R.L. Intensity Calibration and Sensitivity Comparisons for CCD/Raman Spectrometers. *Appl. Spectrosc.* **1993**, *47*, 1965–1974. https://doi.org/10.1366/0003702934066226.
78. McConkey, J.W.; Woolsey, J.M. Errors in Absolute Intensity Measurements Using Tungsten Lamp Standards. *Appl. Opt.* **1969**, *8*, 205. https://doi.org/10.1364/ao.8.000205.
79. Purcell, F.J.; Kaminski, R.; Russavage, E. Radiometric Correction of Raman Spectra. *Appl. Spectrosc.* **1980**, *34*, 323–326.
80. Ray, K.G.; McCreery, R.L. Simplified Calibration of Instrument Response Function for Raman Spectrometers Based on Luminescent Intensity Standards. *Appl. Spectrosc.* **1997**, *51*, 108–116. https://doi.org/10.1366/0003702971938849.
81. *Standard Reference Material 2242a Relative Intensity Correction Standard for Raman Spectroscopy: 532 nm Excitation*; National Institute of Standards and Technology (NIST): Gaithersburg, MD, USA, 2025; pp. 1–5.
82. *Standard Reference Material 2246a Relative Intensity Correction Standard for Raman Spectroscopy: 830 nm Excitation*; National Institute of Standards and Technology (NIST): Gaithersburg, MD, USA, 2022; pp. 1–7.
83. *Standard Reference Material 2244 Relative Intensity Correction Standard for Raman Spectroscopy: 1064 nm Excitation*; National Institute of Standards and Technology (NIST): Gaithersburg, MD, USA, 2020; pp. 1–5.
84. *Standard Reference Material 2241 Relative Intensity Correction Standard for Raman Spectroscopy: 785 nm Excitation*; National Institute of Standards and Technology (NIST): Gaithersburg, MD, USA, 2022; pp. 1–5.
85. *Standard Reference Material 2243 Relative Intensity Correction Standard for Raman Spectroscopy: 488 nm and 514.5 nm Excitation*; National Institute of Standards and Technology (NIST): Gaithersburg, MD, USA, 2009; pp. 1–8.
86. *Standard Reference Material 2245 Relative Intensity Correction Standard for Raman Spectroscopy: 633 nm Excitation*; National Institute of Standards and Technology (NIST): Gaithersburg, MD, USA, 2016; pp. 1–6.
87. Lakowicz, J.R. *Principles of Fluorescence Spectroscopy*; 3rd ed.; Springer New York: New York, NY, USA, 2006; ISBN 978-0-387-31278-1.
88. Iwata, K.; Hamaguchi, H.; Tasumi, M. Sensitivity Calibration of Multichannel Raman Spectrometers Using the Least-Squares-Fitted Fluorescence Spectrum of Quinine. *Appl. Spectrosc.* **1988**, *42*, 12–14. https://doi.org/10.1366/0003702884428608.
89. Melhuish, W.H. Modified Technique for Determining the Wavelength-Sensitivity Curve of a Spectrofluorimeter. *Appl. Opt.* **1975**, *14*, 26–27. https://doi.org/10.1364/AO.14.000026.
90. Raj, A.; Kato, C.; Witek, H.A.; et al. Accurate Intensity Calibration of Multichannel Spectrometers Using Raman Intensity Ratios. *J. Raman Spectrosc.* **2021**, *52*, 2038–2050. https://doi.org/10.1002/jrs.6221.
91. Guo, S.; Kohler, A.; Zimmermann, B.; et al. Extended Multiplicative Signal Correction Based Model Transfer for Raman Spectroscopy in Biological Applications. *Anal. Chem.* **2018**, *90*, 9787–9795. https://doi.org/10.1021/acs.analchem.8b01536.
92. Guo, S.; Heinke, R.; Stöckel, S.; et al. Model Transfer for Raman-Spectroscopy-Based Bacterial Classification. *J. Raman Spectrosc.* **2018**, *49*, 627–637. https://doi.org/10.1002/jrs.5343.
93. Brouckaert, D.; Uyttersprot, J.-S.; Broeckx, W.; et al. Calibration Transfer of a Raman Spectroscopic Quantification Method for the Assessment of Liquid Detergent Compositions from At-Line Laboratory to in-Line Industrial Scale. *Talanta* **2018**, *179*, 386–392. https://doi.org/10.1016/j.talanta.2017.11.025.
94. Myers, N.M.; Gao, B.; Amchin, D.; et al. Calibration Transfer Across Instrument Vendors for Bioprocess Raman Monitoring. *AAPS J.* **2026**, *28*, 1–15. https://doi.org/10.1208/s12248-025-01156-0.
95. Lai, J.; Li, M.; Chen, S.; et al. Calibration Transfer of Deep Learning Models among Multiple Raman Spectrometers via Low-Rank Adaptation. *Anal. Chem.* **2025**, *97*, 19009–19018. https://doi.org/10.1021/acs.analchem.5c01846.
96. Rusu, E.A.; Baia, M. Moving from Raman Spectroscopy Lab towards Analytical Applications: A Review of Interlaboratory Studies. *Instruments* **2023**, *7*, 1–16. https://doi.org/10.3390/instruments7040030.
97. Guo, S.; Beleites, C.; Neugebauer, U.; et al. Comparability of Raman Spectroscopic Configurations: A Large Scale Cross-Laboratory Study. *Anal. Chem.* **2020**, *92*, 15745–15756. https://doi.org/10.1021/acs.analchem.0c02696.
98. Turner, P.; Paton, K.R.; Legge, E.J.; et al. International Interlaboratory Comparison of Raman Spectroscopic Analysis of CVD-Grown Graphene. *2D Mater.* **2022**, *9*, 035010. https://doi.org/10.1088/2053-1583/ac6cf3.